

Film evolution of a spherical soap bubble

David W. Martin · François Blanchette

Received: 23 September 2021 / Accepted: 27 September 2022 / Published online: 15 October 2022 © This is a U.S. Government work and not under copyright protection in the US; foreign copyright protection may apply 2022

Abstract We present a theoretical and numerical study of the time evolution of the film of a soap bubble. Bubbles are assumed to remain approximately spherical with axisymmetric evolution. Inertia is neglected, and the surfactant is assumed insoluble. Applying lubrication theory, we simplify the equations governing the film thickness evolution, surfactant concentration, and tangential fluid velocity. Solving the simplified equations numerically, we examine the long-term behavior of the film and find that most features follow a power law of the form αT^{β} where T is a dimensionless time parameter. We also predict the location (angle from the top) at which the film is thinnest and thus most likely to initiate bursting and present a similarity solution that predicts the decay rate of the minimum film thickness near the pinch-off location.

Keywords Films · Lubrication theory · Navier-Stokes · Surfactant · Thin films

1 Introduction

Soap films are a frequent topic of research in microrheology. Micrometer-scale liquid films are bounded inside and out by much thinner, nanometer-scale layers of surfactants. These surface-active molecules stabilize the film against the influence of gravity and other perturbations. Soap films may be used to accurately determine physical properties of fluids, such as viscosity, surface tension, and surface diffusion [1–4]. They are also the basic component of foams, which have wide-ranging uses in industry [5]. Bursting soap films have been extensively studied in their own right [6–9], but unbroken films tend to yield more information, and we will focus here on their dynamics.

In laboratory studies, soap films are most commonly either planar, being held vertically, or nearly spherical when a free soap film is allowed to form a closed bubble. While plane soap films are often studied for the purpose of understanding 2D turbulence [10–14], we focus here on the dynamics of the more ubiquitous spherical soap bubbles. In a bubble at rest, the fluid within the film drains downward under the influence of gravity while maintaining a horizontally uniform profile when no instabilities are present [15]. Researchers have measured the film thickness as a function of height in an approximately spherical soap bubble using large lateral displacement interferometry [15,16]. A numerical study of the film evolution of anti-bubbles has also been presented [17].

D. W. Martin (⋈)

San Bernardino Valley College, San Bernardino, USA

e-mail: davmartin@valleycollege,edu

F. Blanchette

University of California at Merced, Merced, USA



1 Page 2 of 28 D. W. Martin, F. Blanchette

More recently, researchers have been developing theoretical and numerical methods for tracking film thickness, which have been applied to 3D spherical films. Huang et al. [18] presented a numerical method for tracking non-axially symmetric flow on a spherical bubble and compared their computed effects to experimental observations. Nearly simultaneously, an inviscid model has also been presented for tracking film thickness [19]. We here study theoretically and numerically the dynamics of draining soap bubbles, including viscous effects and focusing on the long-time dynamics that proceed bursting.

To study the time evolution of soap films, we make use of lubrication theory. This method takes advantage of the disparity between the film thickness, usually on the micrometer scale, and the macroscopic scale of the bubble. Lubrication theory has been used extensively in the analysis of thin films [20,21], including films on a solid substrate [22,23], underneath a solid object, subject to gravitational instability [24,25], and free films [26]. In addition to surface tension and body forces, previous studies using lubrication theory have accounted for Van der Waals forces [25], thermocapillarity [27], temperature-dependent viscosity [28], evaporation/condensation [25], and surfactants, soluble [29] or insoluble [30]. Both planar [22,24,26] and cylindrical [31,32] geometries have been analyzed. Lubrication theory was also used to describe flow over a solid sphere [33,34]. An analysis of the drainage at the top of a spherical cap was recently conducted [35], although surfactant sorption and thickness variation effects on the drop curvature were neglected. We present here a more systematic derivation of the governing equations of the drainage of an approximately spherical soap film.

To analyze the film drainage of an approximately spherical soap bubble, we combine theoretical results obtained from lubrication theory and numerical solutions of the resulting partial differential equations. Large-scale shape perturbations are neglected, and the bubble is thus assumed to remain approximately spherical. We also assume that the film profile is axisymmetric as seen from above, an assumption that is often confirmed by observations [15]. For the sake of simplicity, evaporation and airflow are neglected. We also restrict our attention to the regime where the film thickness is small compared to the bubble radius, as is most often the case. Finally, we consider quantities averaged over the film thickness.

We characterize the location (angle with the vertical axis) at which the thickness first tends to zero, corresponding to the most likely location of eventual bursting. We also look at the transient evolution of the film, assuming a uniform initial thickness profile. The thickness profile is the primary quantity of interest, but we also examine the surfactant concentration and tangential velocity profiles on the surface of the film.

The remainder of this paper is organized as follows. In Sect. 2, we apply lubrication theory to simplify the governing equations. After integrating the equations across the film thickness, we incorporate surfactant effects and obtain a reduced system. We then present and validate our numerical method for solving these reduced equations in Sect. 3. Our results for time evolution are presented in Sect. 4, our analysis of the location where the thickness tends to zero is given in Sect. 5, and our similarity solution is presented in Sect. 6. Finally, we present our conclusions in Sect. 7.

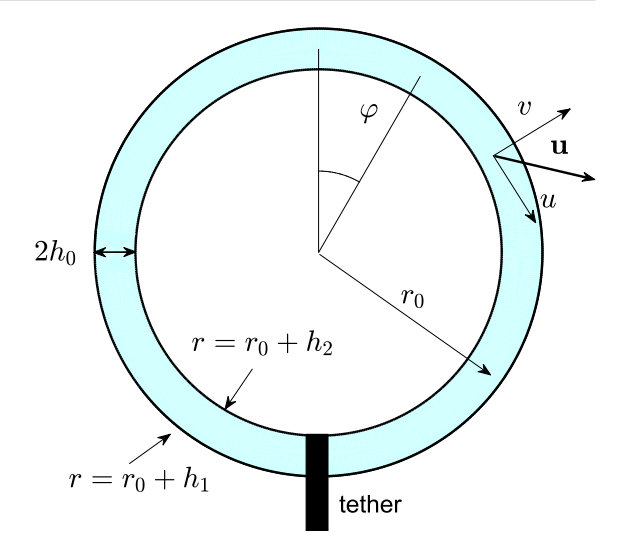
2 Governing equations: lubrication theory

2.1 Physical setup

We consider a stationary bubble, for which air flow is negligible. Thus, air pressure is assumed present, but uniform over the inside and outside surface. This can be achieved by suspending the bubble from the top or bottom, or if the bubble is simply resting on a solid surface, see Fig. 1. In our model, owing to the small thickness of the film, we neglect inertia. Due to symmetry considerations, we impose zero flow at the top and bottom of the bubble, so that the solid object suspending the bubble, if present, does not affect the dynamics of the drainage. We assume the bubble to be approximately spherical—an assumption is valid for small Bond numbers, which we consider here. The radius of the soap bubble, r_0 , is assumed to be much larger than the mean film thickness, $2h_0$. Since the mean film thickness has a micrometer scale, this assumption is valid for $r_0 \ge 10^{-2}$ cm. For simplicity, we consider evaporation to be negligible.



Fig. 1 Schematic of the soap bubbles considered and of the notation used. Note that the figure is not to scale: $\varepsilon = h_0/r_0$ is typically much smaller than shown



In studying the behavior of an approximately spherical soap film, our objective is to obtain integrated equations and solve for the thickness, surface velocity, and surface concentration of surfactants. To this end, we apply lubrication theory, which takes advantage of the disparity in scale between the central bubble radius (average of the inner and outer bubble radii), and the mean film thickness as illustrated in Fig. 1. In particular, we consider $\varepsilon = h_0/r_0 \ll 1$.

2.2 Dimensional equations

We begin with the dimensional axisymmetric incompressible Stokes equations in spherical coordinates [36]:

$$\operatorname{div} \mathbf{u} = \frac{1}{r^2} \frac{\partial}{\partial r} \left(r^2 v \right) + \frac{1}{r \sin \varphi} \frac{\partial}{\partial \varphi} (u \sin \varphi) = 0, \tag{1}$$

$$0 = -\frac{1}{r}\frac{\partial p}{\partial \varphi} + \mu \left(\frac{1}{r^2}\frac{\partial}{\partial r}\left(r^2\frac{\partial u}{\partial r}\right) + \frac{1}{r^2\sin\varphi}\frac{\partial}{\partial \varphi}\left(\sin\varphi\frac{\partial u}{\partial \varphi}\right) - \frac{u}{r^2\sin^2\varphi} + \frac{2}{r^2}\frac{\partial v}{\partial \varphi}\right) - \frac{1}{r}\frac{\partial \varphi}{\partial \varphi},\tag{2}$$

and

$$0 = -\frac{\partial p}{\partial r} + \mu \left(\frac{1}{r^2} \frac{\partial}{\partial r} \left(r^2 \frac{\partial v}{\partial r} \right) + \frac{1}{r^2 \sin \varphi} \frac{\partial}{\partial \varphi} \left(\sin \varphi \frac{\partial v}{\partial \varphi} \right) - \frac{2v}{r^2} - \frac{2}{r^2 \sin \varphi} \frac{\partial}{\partial \varphi} (u \sin \varphi) \right) - \frac{\partial \phi}{\partial r}, \tag{3}$$

where r is the radial coordinate, φ is the angle with the positive vertical axis, u and v are the respective angular and radial components of velocity field, \mathbf{u} , p is the pressure, μ is the viscosity of the fluid in the film, and $\phi = r(\rho - \rho_a)g\cos\varphi$ is a potential associated to a buoyancy force based on the difference between the film density, ρ , and the ambient gas density, ρ_a . We also assume that the normal stress balance between the film and the surrounding air is dominated by surface tension, preserving an approximately spherical bubble.

The fluid has two free surfaces: the exterior surface where $r = r_0 + h_1(\varphi, t)$ and the interior surface where $r = r_0 + h_2(\varphi, t)$, as shown in Fig. 1. To simplify the analysis, we assume that the initial conditions are identical on both the inner and outer interfaces. This will ensure that, to first order, the evolution equations for the surfactant concentration and interface location are identical on both surfaces and their relation to the flow field inside the film is symmetric. In this case, we only need to keep track of a single film surface and we set, $h_1 = -h_2 = h$. Our assumption that the evolution equations are identical for both surfaces is valid only in the limit $\varepsilon \longrightarrow 0$. In the regime we consider, $\varepsilon \ll 1$, typically $\varepsilon \leq 0.01$.

The surface concentration, γ , on the interfaces, satisfies an advection-diffusion equation projected onto the interface [37,38]. However, surface diffusion is usually very small [39–41] and we neglect it, leaving us with

$$\frac{\partial \gamma}{\partial t} + \bar{\nabla}_{s} \cdot (\mathbf{u}_{s} \gamma) = 0, \tag{4}$$



1 Page 4 of 28 D. W. Martin, F. Blanchette

where $\bar{\nabla}_s$ is a gradient operator on the surface. The term $\bar{\nabla}_s \cdot (\mathbf{u}_s \gamma)$ is a divergence projected onto a plane tangent to the interface. Henceforth, we use the subscript s for bulk quantities evaluated on the interface. The usual surface-bulk exchange term [38] is neglected here because we assume the surfactant is insoluble. An examination of the equations governing soluble surfactant is presented in Appendix A.

We describe the effects of the surfactant concentration on the surface tension using the Langmuir equation [37], given in dimensional form as

$$\sigma = \sigma_0 + \mathcal{R}\mathcal{T}\gamma_\infty \log\left(1 - \frac{\gamma}{\gamma_\infty}\right),\tag{5}$$

where \mathcal{R} is the ideal gas constant, \mathcal{T} is the temperature, σ is the surface tension on the interface, and σ_0 is the surface tension of a clean interface.

On the film surface, we first apply a kinematic condition

$$v_{\rm S} = \mathrm{d}h\mathrm{d}t = \frac{\partial h}{\partial t} + \frac{u_{\rm S}}{r} \frac{\partial h}{\partial \varphi}. \tag{6}$$

The stress jump at the boundary is given by the Young-Laplace equation,

$$[\boldsymbol{\tau} \cdot \mathbf{n}]_{\text{film}} - [\boldsymbol{\tau} \cdot \mathbf{n}]_{\text{air}} = -\kappa \sigma \mathbf{n} + \bar{\nabla}_{s} \sigma, \tag{7}$$

where τ is the stress tensor, defined by

$$\boldsymbol{\tau} = \mu(\bar{\nabla}\mathbf{u} + \bar{\nabla}\mathbf{u}') - \mathbf{I}p. \tag{8}$$

Here, the symbol I represents the identity tensor, the prime in $\nabla \mathbf{u}'$ represents a transpose, \mathbf{n} is the outward unit normal, and κ is the total curvature of the interface. We assume the viscosity of the surrounding air to be negligible, so that the stress tensor in the air reduces to $\tau_{\text{air}} = -\mathbf{I}p_{\text{air}}$, and we assume p_{air} to be constant. Note that the air pressure is different on the outside and inside. Because we later differentiate with respect to φ , this will not affect the derivation. The surface gradient can be written

$$\bar{\nabla}_{\mathbf{s}}\sigma = \frac{\partial \sigma}{\partial s}\mathbf{t},$$

where s is arclength along the surface and t is the unit tangent in the direction of increasing arclength.

2.3 Dimensionless equations

We non-dimensionalize our system by writing the radial coordinate as $r = r_0 + h_0 R = r_0 (1 + \varepsilon R)$, where R is a dimensionless rescaled coordinate of order $R = \mathcal{O}(1)$. We leave the angular coordinate, φ , unchanged but let $T = t/t_0$ where $t_0 = \mu r_0/\varepsilon^3 \sigma_0$ is a timescale chosen for reasons to be explained later. We thus define a velocity scale $u_0 = r_0/t_0$ and dimensionless velocity $U = u/u_0$. To balance the continuity equation, and following the usual lubrication theory approach, we scale v using $V = v/\varepsilon u_0$ and obtain a dimensionless continuity equation

$$\frac{\partial V}{\partial R} + \frac{1}{\sin \varphi} \frac{\partial}{\partial \varphi} (U \sin \varphi) = 0. \tag{9}$$

Rescaling the φ momentum equation requires the introduction of a dimensionless parameter. We define a rescaled Bond number, which differs from a standard Bond number by a factor of ε^{-2} , as

$$Bo = \frac{h_0^2(\rho - \rho_a)g}{\mu u_0} = \frac{r_0 h_0(\rho - \rho_a)g}{\sigma_0} \,\varepsilon^{-2}.$$
 (10)

The assumption of spherical geometry breaks down when the non-rescaled Bond number is of order 0.1 or greater, $\varepsilon^2 \text{Bo} \ge \mathcal{O}(0.1)$ [42]. For ordinary soap and water with a micrometer scale film thickness, we have $\rho = 10^3 \, \text{kg/m}^3$, $\rho_a = 1 \, \text{kg/m}^3$, $g = 10 \, \text{m/s}^2$, $\sigma_0 = 0.072 \, \text{N/m}$, and $h_0 = 10^{-6} \, \text{m}$, yielding

$$\varepsilon^2 \text{Bo} = \frac{r_0 (10^{-6} \,\text{m}) (10^3 \,\text{kg/m}^3) (10 \,\text{m/s}^2)}{0.072 \,\text{N/m}} = 0.1,$$



which corresponds to a radius of $r_0 = 0.14$ m and a rescaled Bond number of Bo $\approx 10^9$. We scale the pressure as

$$P = p/p_0$$
 where $p_0 = \frac{u_0 \mu}{h_0 \varepsilon} = \varepsilon \frac{\sigma_0}{r_0}$.

Discarding higher order terms, we obtain from Eq. (2)

$$-\frac{\partial P}{\partial \varphi} + \frac{\partial^2 U}{\partial R^2} + \operatorname{Bo} \sin \varphi = 0. \tag{11}$$

When we rescale the r-momentum equation and discard higher order terms in ε , we obtain from Eq. (3)

$$-\frac{1}{\varepsilon}\frac{\partial P}{\partial R} - \operatorname{Bo}\cos\varphi = 0. \tag{12}$$

We notice that Eq. (12) implies that $\partial P/\partial R = 0$ to leading order. This feature is a common consequence of the lubrication assumption [21].

To obtain a dimensionless surface surfactant evolution equation, we define $\Gamma = \gamma/\gamma_{\infty}$ where γ_{∞} is the maximum packing concentration. Then, if we discard higher order terms, Eq. (4) rescales to

$$\frac{\partial \Gamma}{\partial T} + \frac{1}{\sin \varphi} \frac{\partial}{\partial \varphi} (U_{\rm S} \Gamma \sin \varphi) = 0. \tag{13}$$

Here, $U_s = u_s/u_0$ is the axial velocity projected onto the interface. We note that Eq. (13) was also derived in [43] (Eq. (38)).

The dimensionless form of Eq. (5) is

$$\Sigma = 1 + \text{El}\log\left(1 - \Gamma\right),\tag{14}$$

where

$$El = \frac{\mathcal{R}\mathcal{T}\gamma_{\infty}}{\sigma_0} \tag{15}$$

is an elasticity number and the surface tension has been rescaled as $\Sigma = \sigma/\sigma_0$.

To non-dimensionalize the surface boundary conditions, the rescaled curvature is $K = r_0 \kappa$ and the stress τ is rescaled by pressure given above $\mathbf{T} = \tau/p_0 = \varepsilon^2 r_0 \tau/\mu u_0$. Then, on the outer surface, Eq. (7) has the dimensionless form

$$\mathbf{T} \cdot \mathbf{n} + P_{\text{air}} \mathbf{n} = \frac{1}{\varepsilon} \left(-K \Sigma \mathbf{n} + \frac{\partial \Sigma}{\partial \varphi} \mathbf{t} \right), \tag{16}$$

where $P_{\text{air}} = p_{\text{air}}/p_0$. The capillary number [44] that often appears in Eq. (16) is equal to one due to our choice of timescale: Ca = $\mu u_0/\epsilon^3 \sigma_0 = 1$, which thus justifies our choice of t_0 . On the inner surface, the equation is the same, except for a sign change on the left-hand side. We note that in non-dimensionalizing Eq. (16), we have made the approximation

$$ds = \sqrt{r^2 d\varphi^2 + dr^2} = r_0 \sqrt{d\varphi^2 + \varepsilon^2 dR^2} \sim r_0 d\varphi \quad \text{so} \quad \frac{\partial \Sigma}{\partial s} = \frac{1}{r_0} \frac{\partial \Sigma}{\partial \varphi} + \mathcal{O}(\varepsilon).$$

We introduce the rescaled film thickness as $H = h/h_0 = h/\varepsilon r_0$, a dimensionless quantity of order one. To leading order, at R = H, we thus find that the kinematic condition is

$$V = \frac{\partial H}{\partial T} + U \frac{\partial H}{\partial \varphi},\tag{17}$$

and the curvature is given by

$$K = -2 + \varepsilon \left(\frac{\partial^2 H}{\partial \varphi^2} + \frac{\partial H}{\partial \varphi} \cot \varphi + 2H \right) \tag{18}$$

(see Eq. (71) in Appendix B). Taking the dot product of Eq. (16) with the unit normal and keeping only terms of order one or greater, we find that the normal stress balance at R = H is

$$P - P_{\text{air}} = \Sigma \left(\frac{2}{\varepsilon} - \frac{\partial^2 H}{\partial \varphi^2} - \frac{\partial H}{\partial \varphi} \cot \varphi - 2H \right). \tag{19}$$

1 Page 6 of 28 D. W. Martin, F. Blanchette

At R = -H the stress balance is similar, with the coefficients of terms involving H changing sign. The tangential stress balance is

$$\frac{\partial U}{\partial R} = \frac{1}{\varepsilon^2} \frac{\partial \Sigma}{\partial \varphi}.$$
 (20)

A detailed derivation of Eqs. (19) and (20) is presented in Appendix B.

2.4 Additional symmetry conditions

As a consequence of the symmetry of the problem, we can also impose symmetry in the bulk liquid at the center of the film where R = 0, which gives, in dimensionless form,

$$V\big|_{R=0} = 0$$
 and $\frac{\partial U}{\partial R}\Big|_{R=0} = 0.$ (21)

At the rotation axis, where $\varphi = 0$ or π , we also impose symmetry boundary conditions:

$$U\big|_{\varphi=0,\pi} = \frac{\partial \Gamma}{\partial \varphi}\bigg|_{\varphi=0,\pi} = \frac{\partial H}{\partial \varphi}\bigg|_{\varphi=0,\pi} = 0. \tag{22}$$

Finally, the system has initial condition

$$H\big|_{T=0} = H_i(\varphi). \tag{23}$$

We do not require initial conditions on U_s and Γ , as they are determined entirely by H, as we explain in more detail in Sects. 2.5 and 3.1.

2.5 Flow equations integrated across the film

To simplify the system of equations further, we eliminate the dependence on R by integrating across the film, in a manner similar to what is done on a flat surface to derive the shallow water equations [45] and in a way often used to describe flow in thin films [39,51]. Beginning with the continuity Eq. (9) and defining a total flux in the film, in spherical coordinates, $Q = \sin \varphi \int_0^H U \, dR$, we integrate over the half-thickness of the film (the other half is identical by symmetry),

$$\frac{\partial H}{\partial T} + \frac{1}{\sin \alpha} \frac{\partial Q}{\partial \alpha} = 0. \tag{24}$$

Now, we integrate Eq. (11) twice, applying relevant boundary conditions (21) to find a parabolic flow profile

$$U = \frac{1}{2}(R^2 - H^2)\left(\frac{\partial P}{\partial \varphi} - \operatorname{Bo}\sin\varphi\right) + U_{s}(T,\varphi). \tag{25}$$

Here, $U_s = u_s/U_0$ is the axial velocity projected onto the interface. We integrate again to get an expression for the flux

$$Q = \left(-\frac{1}{3}H^3\left(\frac{\partial P}{\partial \varphi} - \operatorname{Bo}\sin\varphi\right) + HU_{s}(T,\varphi)\right)\sin(\varphi). \tag{26}$$

Equations (24) and (26) can now be combined to form a thickness evolution equation:

$$\frac{\partial H}{\partial T} + \frac{1}{\sin \varphi} \frac{\partial}{\partial \varphi} \left(\left(-\frac{1}{3} H^3 \left(\frac{\partial P}{\partial \varphi} - \operatorname{Bo} \sin \varphi \right) + H U_{s}(T, \varphi) \right) \sin \varphi \right) = 0. \tag{27}$$



2.6 Surfactant effects

To simplify the stress condition, we substitute Eq. (14) into Eq. (20) and obtain

$$\left. \frac{\partial U}{\partial R} \right|_{s} = \frac{\mathrm{El}}{\varepsilon^{2}} \frac{\partial}{\partial \varphi} \log(1 - \Gamma) = \mathrm{Mg} \frac{\partial}{\partial \varphi} \log(1 - \Gamma), \tag{28}$$

where we have defined a Marangoni number:

$$Mg = \frac{El}{\varepsilon^2}.$$
 (29)

We see from Eq. (29) that if Mg = $\mathcal{O}(1)$, then El = $\mathcal{O}(\varepsilon^2) \ll 1$, which means that the surfactant has negligible effect on surface tension. In that case, unless Γ approaches 1, a regime we do not consider here, a Taylor expansion of Eq. (14) yields $\Sigma = 1 + \mathcal{O}(\varepsilon^2)$ implying that to first order $\Sigma = 1$. Our assumption of constant Σ breaks down only when $\Gamma \geq 1 - \exp(\varepsilon^{-2})$. When inserted into Eq. (14), we obtain variations of $\mathcal{O}(1)$ in Σ . In other words, even though the surfactant coverage of the surface hardly impacts the overall surface tension, it still remains at a level such that Marangoni stresses can balance viscous shear stresses given the flow that develops within the film. This confirms that, to first order, the pressure within the film is constant, ensuring that the normal stress balance is satisfied when the curvature is also constant, which is to say when the bubble is spherical with a pressure difference between the inner and outer air of $P_{\text{air,in}} - P_{\text{air,out}} = 4\Sigma/\varepsilon$. We hence substitute Eq. (19) into Eq. (27) to get

$$\frac{\partial H}{\partial T} + \frac{1}{\sin\varphi} \frac{\partial}{\partial\varphi} \left(\left(\frac{1}{3} H^3 \frac{\partial}{\partial\varphi} \left(\frac{\partial^2 H}{\partial\varphi^2} + \frac{\partial H}{\partial\varphi} \cot\varphi + 2H \right) + \frac{1}{3} H^3 \operatorname{Bo} \sin\varphi + H U_{\mathrm{s}}(T,\varphi) \right) \sin\varphi \right) = 0. \tag{30}$$

We note that multiplying by $1/\sin\varphi$ does not lead to any singularity at the axis, because $\partial H/\partial\varphi=0$ there. Other authors have presented an equation similar to (30), as a continuity equation, but without the gravitational and nonlinear terms (see [43, Eq. 30]). Rather, the gravitational term was introduced in a momentum balance equation. From there, the resulting system of equations is very different from ours, and is not applicable to the regime where our rescaled Bond number is of order one.

Similarly, we can combine equation (28) and the radial derivative of (25), to find

$$\operatorname{Mg} \frac{\partial}{\partial \varphi} \log(1 - \Gamma) = H \left(\frac{\partial P}{\partial \varphi} - \operatorname{Bo} \sin \varphi \right).$$

Finally, we substitute in Eq. (19) to get

$$\operatorname{Mg} \frac{\partial}{\partial \varphi} \log(1 - \Gamma) = -H \left(\frac{\partial}{\partial \varphi} \left(\frac{\partial^2 H}{\partial \varphi^2} + \frac{\partial H}{\partial \varphi} \cot \varphi + 2H \right) + \operatorname{Bo} \sin \varphi \right). \tag{31}$$

Together, Eqs. (30), (31), and (13) comprise a system of three equations with three unknowns: Γ , U_s , H. Eq. (30) enforces conservation of fluid mass, while Eq. (13) conserves surfactant mass. Eq. (31) is a boundary condition that relates Γ to H. There is no evolution equation for U_s , which only appears in (13), and therefore, this equation is used to determine U_s , while Eq. (31) can be used to determine Γ , and Eq. (30) can be used to advance H in time. We note that in Appendix A, we have extended our governing equations to include sorption effects.

3 Numerical method and validation

This system of equations (30), (31), and (13), admits no steady-state solution (see Sect. 5), so that the bubble always eventually bursts. We consider two separate regimes. The first is the limit of large Marangoni number, $Mg \gg 1$. The second is $Bo \in [1, 10]$, $Mg \in [2, 10]$, and $\bar{\Gamma} \in [0.5, 0.9]$. Here, $\bar{\Gamma}$ is the average surfactant concentration on the surface as a fraction of the maximum possible concentration.



1 Page 8 of 28 D. W. Martin, F. Blanchette

3.1 Initial condition

To determine the behavior over time, we supply the initial condition $H(0, \varphi) = 1$, chosen for simplicity, and advance the system in time numerically. We have also looked at the initial condition $H(0, \varphi) = 1 - 0.9 \cos \varphi$ for comparison, and found the long-time evolution to be similar. Because of Eq. (31), the surfactant profile is determined entirely by the thickness profile, H. Thus, it is not possible in our model to have both H and Γ initially uniform. In cases where sorption, i.e., transfer of surfactant between the bulk and the interface, is present, a broader range of initial conditions should be feasible, but our assumption on insoluble surfactant limits the possible initial conditions.

In the case Mg \gg 1, where the dominant balance is between Marangoni stresses and gravity, the system can develop the necessary Marangoni stresses to enforce $H(0,\varphi)=1$ and a non-uniform surfactant profile on the surface, such as we impose. However, for Mg \in [2, 10], it is more likely that the dominant balance is between the curvature term and gravity, in which case the rapid evolution will be toward an uneven thickness profile, and the initial condition $H(0,\varphi)=1$ is less likely to be physical. This explains why we do not find initial surfactant concentration profiles consistent with $H(0,\varphi)=1$ for Mg $=\mathcal{O}(1)$.

3.2 Large Marangoni number limit

In the regime where Mg \gg 1, we can expand the variables in powers of Mg⁻¹ and obtain $\Gamma = \bar{\Gamma}$ and $U_s = 0$, to leading order (see Appendix C). Physically, this means that Marangoni stresses will quickly even out the surfactant distribution on the surface and thus suppress tangential flows. To describe this regime, we define a new Bond number and timescale based on the equilibrium, rather than surfactant-free, surface tension $\sigma_{eq} = \sigma_0 \left(1 + \text{El} \log(1 - \bar{\Gamma})\right)$. Specifically,

$$Bo_{eq} = \frac{r_0 h_0 (\rho - \rho_a) g}{\sigma_{eq}} \varepsilon^{-2}$$
(32)

and $\bar{T} = t/t_{\rm eq}$ where $t_{\rm eq} = \mu r_0/\varepsilon^3 \sigma_{\rm eq}$. Note that the definitions of the elasticity number and Marangoni number remain the same. We then obtain a simplified, and decoupled, film thickness evolution equation:

$$\frac{\partial H}{\partial \bar{T}} + \frac{1}{\sin \varphi} \frac{\partial}{\partial \varphi} \left(\frac{1}{3} H^3 \left(\frac{\partial}{\partial \varphi} \left(\frac{\partial^2 H}{\partial \varphi^2} + \frac{\partial H}{\partial \varphi} \cot \varphi + 2H \right) + \operatorname{Bo}_{\text{eq}} \sin \varphi \right) \sin \varphi \right) = 0. \tag{33}$$

To solve Eq. (33), we discretize it in space using second-order finite differences. Due to stability considerations and the fact that the equation is fourth order, we set $\Delta T \propto (\Delta \varphi)^4$. We advance the system in time using an explicit Euler time-stepping method. Simulation results are presented in Sect. 4.1.

3.3 Intermediate Marangoni number: $Mg \in [2, 10]$

To solve numerically equations (30), (31), and (13) in terms of Γ , U_s , and H, we discretize Eq. (30) in the same way as Eq. (33)—using finite differences in space and an explicit Euler method in time. Next, we solve Eq. (31) for Γ :

$$\Gamma = 1 - c_{\Gamma}(T)e^{I(T,\varphi)} \quad \text{where} \quad I(T,\varphi) = -\frac{1}{\text{Mg}} \int_{0}^{\varphi} H\left(\frac{\partial}{\partial \psi} \left(\frac{\partial^{2} H}{\partial \psi^{2}} + \frac{\partial H}{\partial \psi} \cot \psi + 2H\right) + \text{Bo} \sin \psi\right) d\psi. \quad (34)$$

Here, $c_{\Gamma}(T)$ is a constant of integration that we determine based on the total surfactant mass, M_{Γ} , which, in the absence of sorption, i.e., surfactant interchange between the bulk and the surface, is constant. In particular, we have

$$M_{\Gamma} = 4\pi \,\bar{\Gamma} = 2\pi \,\int_{0}^{\pi} \left(1 - c_{\Gamma}(T) \mathrm{e}^{I(T,\varphi)}\right) \sin\varphi \,\mathrm{d}\varphi,$$

where $\bar{\Gamma}$ is the average surfactant concentration on the surface. Solving for c_{Γ} , we obtain

$$c_{\Gamma}(T) = \frac{2 - 2\bar{\Gamma}}{\int_0^{\pi} e^{I(T,\varphi)} \sin \varphi \, d\varphi}.$$
 (35)



Table 1 Limiting surfactant concentrations ensuring that the initial dimensionless surfactant concentration is between zero and one for various Bond/Marangoni number ratios

Bo/Mg	$\Gamma_{ m min}$
0	0
0.1	0.0937
0.5	0.3679
1	0.5677
1.5	0.6833
2	0.7546
5	0.9000
10	0.9500
∞	1

Because we non-dimensionalized Γ using the maximum surfactant concentration, we require $0 \le \Gamma \le 1$, which adds a constraint on $\bar{\Gamma}$. If we initially set H = 1, then the curvature terms vanish, in which case

$$I(0,\varphi) = \frac{\mathrm{Bo}}{\mathrm{Mg}}(\cos\varphi - 1) \quad \text{and} \quad \int_0^\pi \mathrm{e}^{I(0,\varphi)}\sin\varphi \; \mathrm{d}\varphi = \frac{\mathrm{Mg}}{\mathrm{Bo}}(1 - \mathrm{e}^{-2\mathrm{Bo}/\mathrm{Mg}}),$$

where the ratio Bo/Mg captures the importance of the gravitational force relative to that of Marangoni forces. Hence,

$$c_{\Gamma}(T=0) = \frac{2\text{Bo}}{\text{Mg}} \frac{1 - \bar{\Gamma}}{1 - e^{-2\text{Bo/Mg}}},$$
 (36)

and altogether we have

$$\Gamma(0,\varphi) = 1 - \frac{2\text{Bo}}{\text{Mg}} \frac{1 - \bar{\Gamma}}{1 - e^{-2\text{Bo}/\text{Mg}}} e^{\text{Bo}(\cos\varphi - 1)/\text{Mg}}.$$
 (37)

Imposing $0 \le \Gamma \le 1$, or equivalently $0 \le c_{\Gamma} e^{I(0,\varphi)} \le 1$, yields the condition

$$0 \leq \frac{2Bo}{Mg} \frac{1 - \bar{\Gamma}}{1 - e^{-2Bo/Mg}} e^{(\cos \varphi - 1)Bo/Mg} \leq 1.$$

From here, we use the fact that $\cos \varphi - 1 \le 0$ and $Bo/Mg \ge 0$, so that $0 \le e^{(\cos \varphi - 1)Bo/Mg} \le 1$. We are left with the condition that

$$\bar{\Gamma} \ge 1 - \frac{1 - e^{-2Bo/Mg}}{2Bo/Mg} \equiv \Gamma_{min}.$$
 (38)

In a physical system where this condition is not met, our chosen initial condition H=1 is not possible. We show in Table 1 limiting surfactant concentrations and associated rescaled Bond/Marangoni number ratios, and in Fig. 2 plots of $\Gamma(0, \varphi)$ for various values of Bo/Mg and $\bar{\Gamma}$.

For an initial average concentration above Γ_{\min} , we may solve Eq. (13) for U_s and find

$$U_{\rm S}(T,\varphi) = -\frac{1}{\Gamma \sin \varphi} \int_0^{\varphi} \frac{\partial \Gamma}{\partial T} \sin \psi \, \mathrm{d}\psi. \tag{39}$$

The lower bound of integration has been chosen so that $U_s(T, 0) = 0$ and the condition $U_s(T, \pi) = 0$ is imposed separately. Note that imposing those conditions ensures that we never use Eq. (39) when $\sin \varphi = 0$, thus avoiding issues associated with dividing by zero.

Because the time step is much smaller than $\Delta \varphi$, the time derivative $\partial \Gamma / \partial T$ is unstable if computed at every time step. We avoid this problem by computing the time derivative of Γ over a time span of $\Delta T_2 = \Delta \varphi$:

$$\frac{\partial \Gamma}{\partial T}\Big|_{T=T_0} \approx \frac{\Gamma(T_0 + \Delta T_2, \varphi) - \Gamma(T_0, \varphi)}{\Delta T_2} = \frac{\Gamma(T_0 + \Delta \varphi, \varphi) - \Gamma(T_0, \varphi)}{\Delta \varphi}.$$

Page 10 of 28 D. W. Martin, F. Blanchette

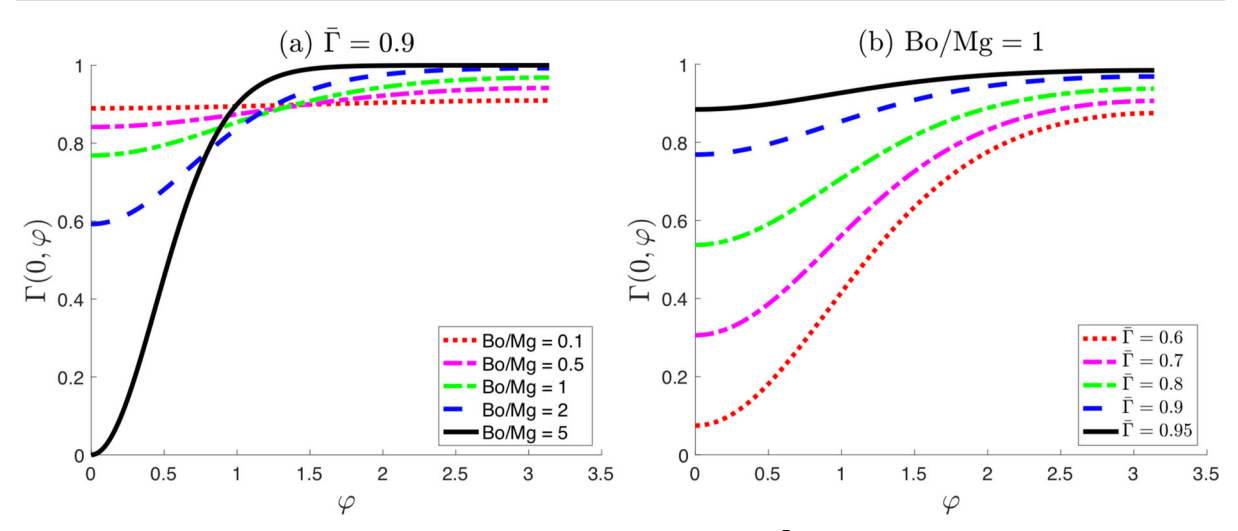


Fig. 2 Initial surfactant concentration as a function of the angle from the top, φ , for $\bar{\Gamma}=0.9$ and various values of Bo/Mg (a) and for Bo/Mg = 1 and various values of $\bar{\Gamma}$ (b)

We verified that our method is robust against the choice of ΔT_2 . In particular, using $\Delta T_2 = 2\Delta \varphi$ or $\Delta T_2 = 0.5\Delta \varphi$ resulted in surface velocities that differed by less than 0.6% from the case with $\Delta T_2 = \Delta \varphi$ for all times greater than zero. Differences in Γ and H were even smaller.

The initial surface velocity $U_s(0,\varphi)=U_{s,i}$ appears in both Eqs. (30) and (39) and both equations must therefore be solved simultaneously to obtain a consistent initial condition, $U_{s,i}$. We do so by solving each equation in turn in an iterative manner, beginning with the assumption that $U_{s,i}=0$. First, we solve Eq. (30) for H with $U_{s,i}$ set to zero. Then, we solve Eq. (31) for Γ . Calculating Γ at different times, we obtain $\partial \Gamma/\partial T$, which we insert into Eq. (39) to solve for $U_{s,i}$. We then reset Γ and H to their known initial values every time we update $U_{s,i}$. When $U_{s,i}$ converges, we have obtained the initial surface velocity, $U_{s,i}$. The convergence of $U_{s,i}$ depends on the Bond number, the Marangoni number, and the average surfactant concentration. For Bo = 1, Mg = 10, and $\Gamma = 0.9$, convergence is very rapid—occurring in as few as 3 iterations. When Bo = 1, $\Gamma = 0.9$, as Mg approaches approximately 1.5, the number of iterations increases without bound, and for values of Mg below approximately 1.5, convergence fails. Similarly, when Bo = 1, convergence fails for $\Gamma < 0.5$, for all values of Mg. In those cases, our assumed initial condition, H = 1, is not feasible, and we therefore focus on the regime where Mg ≥ 2 and $\Gamma \geq 0.5$. The initial condition can be sensitive to numerical parameters, but we verified that the long-term behaviors ($T \geq 1$), which is what we focus on, are not.

3.4 Validation

We present here results confirming that convergence is achieved in terms of both temporal and spatial discretizations. We also validate our method by showing conservation of film and surfactant mass, and by comparing our results to existing experimental results.

We first consider spatial resolution for the case when Mg $\gg 1$, the change of thickness at the top of the drop was found to vary by less than 0.0012% when simulations were performed with $\Delta \varphi = 0.01$ compared to $\Delta \varphi = 0.02$, taken at T=10, confirming that results are well resolved with $\Delta \varphi = 0.02$, a value we use in the remainder of our study. We next consider spatial resolution for the case when Bo = 1, Mg = 10, and $\bar{\Gamma} = 0.9$. Here, $\bar{\Gamma}$ is the mean surfactant concentration on the surface. We measure the relative variation in thickness at the top of the drop, the variation in surface surfactant concentration at the top of the drop relative to $\bar{\Gamma} = 0.9$, and the relative variation in maximum absolute surface velocity. We thus define errors as



Resolutions	err_H	$\operatorname{err}_{\Gamma}$	err_U
$\Delta \varphi = 0.04$	6×10^{-3}	1.8×10^{-4}	4×10^{-3}
$\Delta \varphi = 0.02$	6.1×10^{-4}	2.6×10^{-5}	3.9×10^{-4}

Table 3 Relative errors for two pairs of temporal meshes at time T=10, with Bo = 1, Mg = 10, and $\bar{\Gamma}=0.9$, compared against $\Delta T_2=0.01$

Resolutions	$E_{ m H}$	E_{Γ}	$E_{ m U}$
$\Delta T = 8 \times 10^{-9}, \Delta T_2 = 0.04$	5.2×10^{-6}	2.1×10^{-8}	2.3×10^{-3}
$\Delta T = 4 \times 10^{-9}, \Delta T_2 = 0.02$	2.6×10^{-6}	1.1×10^{-8}	1.1×10^{-3}

$$\operatorname{err}_{H} = \frac{|H_{\operatorname{coarse}}(T,0) - H_{\operatorname{fine}}(T,0)|}{H_{\operatorname{fine}}(T,0)},$$

$$\operatorname{err}_{\Gamma} = \frac{|\Gamma_{\operatorname{coarse}}(T,0) - \Gamma_{\operatorname{fine}}(T,0)|}{\bar{\Gamma}},$$
and
$$\operatorname{err}_{U} = \frac{|U_{\operatorname{s,max,coarse}}(T) - U_{\operatorname{s,max,fine}}(T)|}{U_{\operatorname{s,max,fine}}(T)}.$$

$$(40)$$

Here, quantities subscripted "coarse" are evaluated on the coarser of the two grids and quantities subscripted "fine" are evaluated on the finer of the two grids, while $U_{s,max,coarse}$ and $U_{s,max,fine}$ are the maximum absolute surface velocity on the coarser and finer grids, respectively. Table 2 shows better than second-order convergence, and good accuracy for $\Delta \varphi = 0.02$.

We also tested three temporal resolutions for the case when Mg \in [2, 10]. Keeping $\Delta T = 2 \times 10^{-5} \Delta T_2$, we consider $\Delta T_2 = 0.04$, 0.02, and 0.01. We defined relative error at time T for H, Γ , and U_s , respectively, to be

$$E_{H} = \max_{\varphi \in [0,\pi]} \frac{|H_{\text{coarse}}(T,\varphi) - H_{\text{fine}}(T,\varphi)|}{H_{\text{fine}}(T,\varphi)},$$

$$E_{\Gamma} = \max_{\varphi \in [0,\pi]} \frac{|\Gamma_{\text{coarse}}(T,\varphi) - \Gamma_{\text{fine}}(T,\varphi)|}{\bar{\Gamma}},$$
and
$$E_{U} = \max_{\varphi \in [0,\pi]} \frac{|U_{\text{s,coarse}}(T,\varphi) - U_{\text{s,fine}}(T,\varphi)|}{U_{\text{s,max,fine}}(T)}.$$

$$(41)$$

The results at time T=10, given in Table 3, show first-order convergence for H, Γ , and U_s . All convergence results were obtained using Bo = 1, Mg = 10, and $\bar{\Gamma}=0.9$. Based on these results, we conclude that time steps of $\Delta T=4\times 10^{-9}$ and $\Delta T_2=0.02$ provide sufficient accuracy and the results we present later were obtained with these time steps.

We also validated our conservation of film mass and surfactant mass. We measure variation in surfactant mass by computing the quantity

$$\Delta M_{\Gamma} = \frac{|M_{\Gamma}(100) - M_{\Gamma}(0)|}{M_{\Gamma}(0)}, \quad \text{where} \quad M_{\Gamma}(T) = 2\pi \int_0^{\pi} \Gamma(T, \varphi) \sin \varphi \, \mathrm{d} \varphi$$

is the total surfactant mass at time T. Table 4 shows ΔM_{Γ} for various parameter values. In all cases, $\Delta M_{\Gamma} \leq 10^{-5}$. Similar to the surfactant mass, we measure variations in film mass by computing the quantity

$$\Delta M = \frac{|M(100) - M(0)|}{M(0)}, \text{ where } M(T) = 8\pi \int_0^{\pi} H(T, \varphi) \sin \varphi \, \mathrm{d}\varphi$$



1 Page 12 of 28 D. W. Martin, F. Blanchette

Table 4	Variations in	surfactant	mass for different	cases at time T	' = 10

Case			ΔM_{Γ}
Bo = 1	Mg = 10	$\bar{\Gamma} = 0.9$	5.274×10^{-7}
Bo = 1	Mg = 2	$\bar{\Gamma} = 0.9$	2.995×10^{-6}
Bo = 1	Mg = 10	$\bar{\Gamma}=0.5$	4.744×10^{-6}
Bo = 10	Mg = 10	$\bar{\Gamma} = 0.9$	7.140×10^{-6}

Fig. 3 Thickness profile against the vertical displacement from the center. Here, $Mg = \infty$

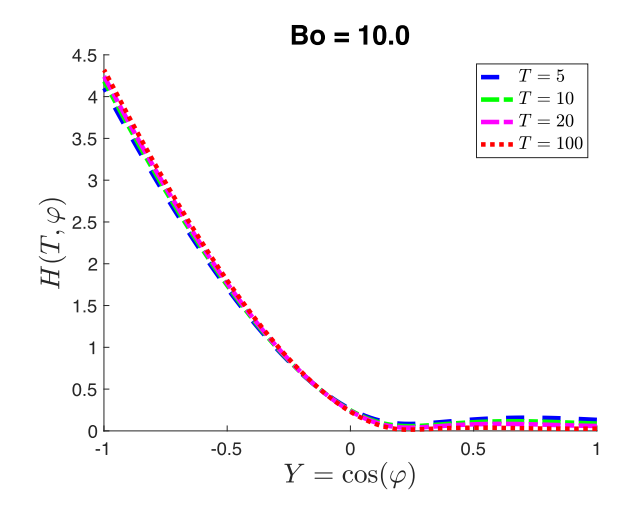


Table 5 Variations in film mass for different cases at time T = 10

Case			ΔM	
Bo = 1	Mg = 10	$\bar{\Gamma} = 0.9$	2.136×10^{-4}	
Bo = 1	Mg = 2	$\bar{\Gamma} = 0.9$	2.136×10^{-4}	
Bo = 1	Mg = 10	$\bar{\Gamma} = 0.5$	2.136×10^{-4}	
Bo = 10	Mg = 10	$\bar{\Gamma} = 0.9$	4.757×10^{-4}	

is the total film mass at time T. Table 5 shows ΔM for various parameters covering the regime studied in Sect. 4. In all cases, $\Delta M \le 5 \times 10^{-4}$.

Finally, we compare qualitatively our thickness profile, $H(\varphi, T)$ at different times to published experimental results. For the case of infinite Marangoni number and a Bond number of Bo = 10, shown as the dashed line in Fig. 3, we observe qualitatively similar behavior to that reported in [15, Fig. 9] and [16, Fig. 3(a)]. We also note that dimpling occurs in the thickness profile, similar to what has been observed in [46,47]. However, the dimpling in those cases occurred without the influence of gravity, whereas the dimpling in the present study is dependent on gravitational effects (see Sect. 5). In general, a quantitative comparison is not possible, due to the different definitions of the governing parameters, specifically the rescaled Bond number.

4 Time evolution of the system

We consider first the limit of large Marangoni number where the only independent parameter remaining is the rescaled equilibrium Bond number, Bo_{eq} . In that case, we focus on the time evolution of H, the only quantity that is not rendered uniformly constant. We then study the more complicated regime where $Mg \in [2, 10]$ and Bo is of



Table 6 Fitted coefficients and powers for H_{min}

Bo _{eq}	α	β
1	0.34	-0.62
2	0.26	-0.56
3	0.23	-0.53
4	0.22	-0.52
5	0.22	-0.53
6	0.23	-0.55
10	0.23	-0.60
15	0.19	-0.60
20	0.16	-0.58
25	0.13	-0.55

The curve fitting is done for times $50 \le \bar{T} \le 100$

order one. We vary three independent parameters, Bo, Mg, and $\bar{\Gamma}$, and examine the three dependent parameters, $H(T, \varphi), \Gamma(T, \varphi), \text{ and } U_s(T, \varphi).$

4.1 Large Marangoni number limit: results

We ran simulations of Eq. (33) beginning with $H(0,\varphi)=1$, and over the range $\bar{T}\in[0,100]$. Our results for various Bond numbers are shown in Fig. 4. Fluid drains from the top portion of the bubble and accumulates at the bottom, so that two distinct regions appear: a top region where $H \ll 1$, and a bottom region where H is of order 1. These regions are separated by a local minimum in the thickness profile. In all cases, at long enough time, the time derivative of H decreases toward zero for all values of φ , and H does not reach zero in finite time.

We note that the thinnest part of the film is not at the top, but at some critical angle, φ_c , along the profile of the film (see Fig. 5). This can be explained by the fact that the drainage of the film is driven by gravity, and is proportional to $\sin \varphi$ (see Eq. (11)). Gravitational effects therefore go to zero and the bottom and, more importantly, at the very top of the bubble, which pushes the thinnest part of the film off the symmetry axis. We note that the top part of the film remains much thinner than the bottom portion of the film, due to the cumulative effect of the drainage.

To gauge the time evolution of the system, we track the minimum thickness, $H_{\min}(\bar{T})$, as a function of time. Figure 6a shows the time decay of $H_{\min}(\bar{T})$. We see that larger values of Bo_{eq} result in a faster decrease of the minimum thickness, as gravitational effects accelerate the film drainage. The log-log plots of $H_{\min}(T)$ are approximately linear for Bo_{eq} ≥ 1 which suggests a relation of the form $H_{\min}(\bar{T}) = \alpha \bar{T}^{\beta}$. The resultant values for α and β obtained using least squares regression on $\bar{T} \in [50, 100]$ are given in Table 6. The fitted curves shown in Fig. 6b show good agreement with the computed curves for sufficiently large times. The values of α and β exhibit non-monotonic behavior at intermediate values of Bo_{eq}. We note that these results are for intermediate times, $T \in [50, 100]$, only. In the limit as $\bar{T} \longrightarrow \infty$, the exponents may change. In this limit, however, other factors not included here are likely to be determinant, notably the disjoining pressure [48].

4.2 An intermediate Marangoni number of Mg \in [2, 10]

To describe this regime, we ran simulations of the time evolution of Eqs. (30), (34), and (39) for different rescaled Bond numbers, Marangoni numbers, and average surfactant concentrations, Γ, tracking the thickness profile, $H(T,\varphi)$, surfactant concentration on the surface, $\Gamma(T,\varphi)$, and fluid velocity on the surface, $U_s(T,\varphi)$.



Page 14 of 28 D. W. Martin, F. Blanchette

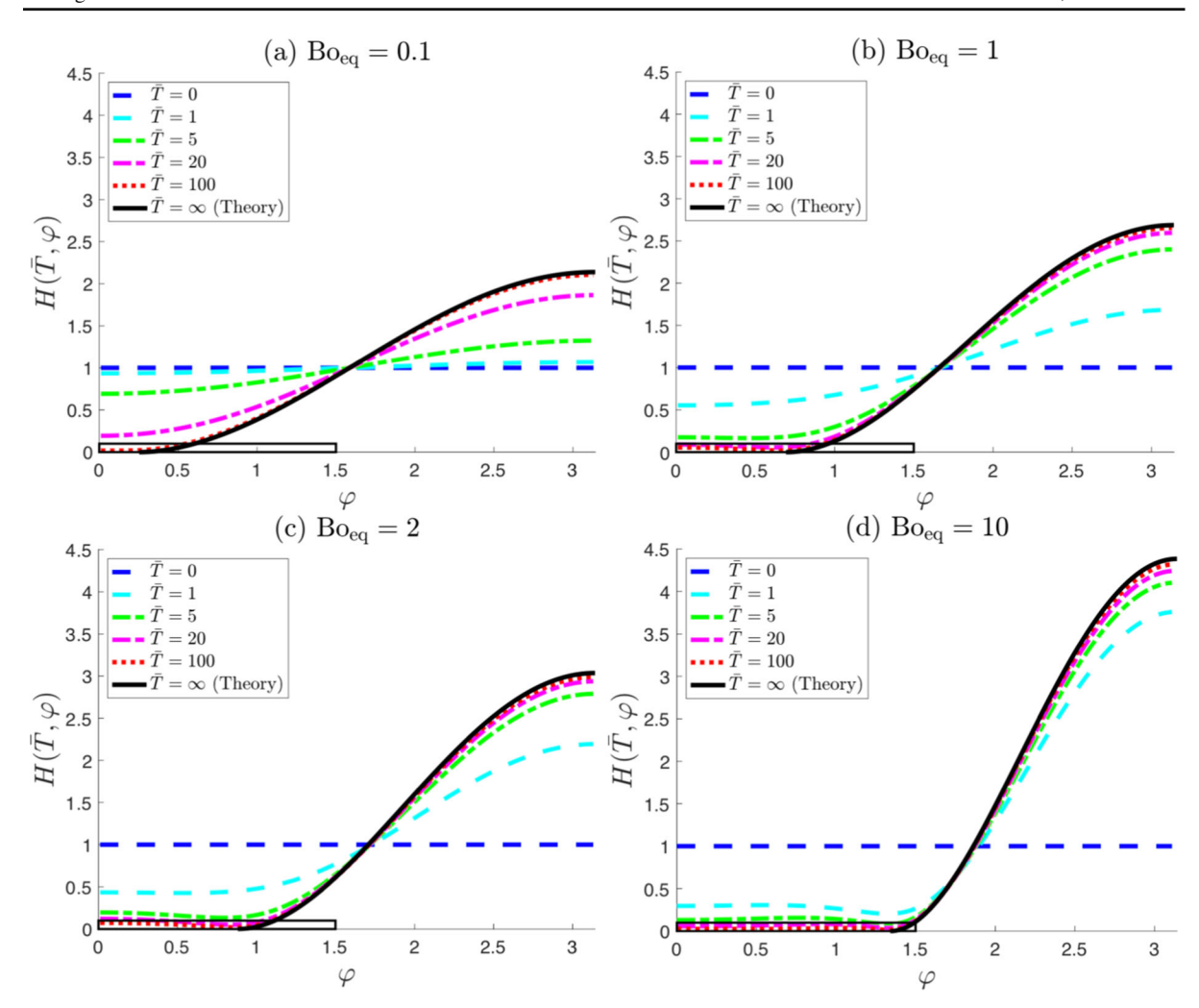


Fig. 4 Half-thickness of the film, H, as a function of the angle from the top, φ , at various times obtained by solving Eq. (33), for four different rescaled Bond numbers. The black curves are obtained as described in Sect. 5, using Eqs. (46) and (47). The rectangles indicate the extent of the zoomed-in regions shown in Fig. 5 which demonstrate that the thickness exhibits a local (and global) minimum at $0 < \varphi_c < \pi$

Figure 7 shows the time evolution of the system for Mg = 2, $\bar{\Gamma}$ = 0.9, and Bo = 1. The time evolution of $H(T,\varphi)$ is nearly identical to the case Mg \gg 1 studied in Sect. 4.1 with plots that are visibly indistinguishable for different values of Mg and $\bar{\Gamma}$. This is because the surface velocity is relatively small for all cases studied, with values ranging from 10^{-4} to 2×10^{-2} . Hence, Eq. (30) differs only by a small term from Eq. (33).

The surfactant concentration on the surface, $\Gamma(T, \varphi)$, begins with a non-uniform distribution to allow for a uniform initial value of H, as described by Eq. (37). It then relaxes toward a uniform distribution $\Gamma(T, \varphi) \longrightarrow \bar{\Gamma}$ as $T \longrightarrow \infty$. The initial surfactant gradients can be scaled by

$$\Delta\Gamma_0 = \max_{\varphi \in [0,\pi]} \Gamma(0,\varphi) - \min_{\varphi \in [0,\pi]} \Gamma(0,\varphi) = \Gamma(0,\pi) - \Gamma(0,0) = \frac{2\mathrm{Bo}}{\mathrm{Mg}} \left(1 - \bar{\Gamma}\right),\tag{42}$$

where the last equality comes from Eq. (37). This initial relationship matches physical intuition. In particular, we expect drainage to occur faster for increasing Bo, leading to larger initial surfactant gradients. For increasing Mg, we expect that the surfactant concentration will be more uniform initially, resulting in lower values of $\Delta\Gamma_0$. For



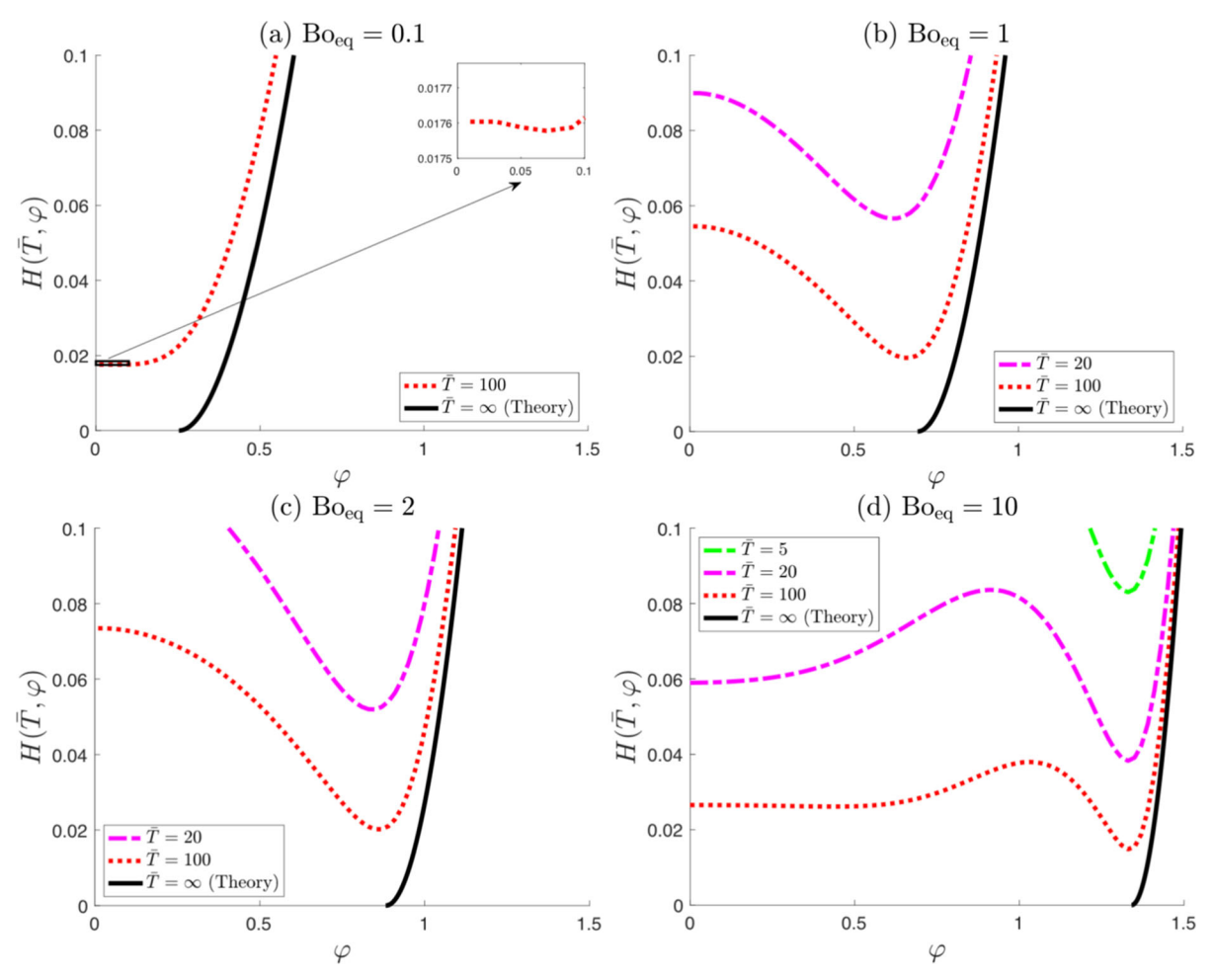


Fig. 5 Closeups of the half-thickness of the film, H, as a function of the angle from the top, φ , at various times obtained by solving Eq. (33), for four different rescaled Bond numbers shown more broadly in Fig. 4. The black curve is obtained in Sect. 5, using Eqs. (46) and (47). The inset in **a** shows a closeups of the curve near zero

increasing $\bar{\Gamma}$, we know from Eq. (37) that $\Gamma(0, \varphi)$ is be confined to a narrower range of values, resulting in lower surfactant gradients.

The time decay of the variations in surfactant concentration can be measured by the time decay of the normalized change in surfactant across the film

$$\Delta\Gamma_{\mathrm{rel}}(T) = \frac{1}{\Delta\Gamma_0} \left(\max_{\varphi \in [0,\pi]} \Gamma(T,\varphi) - \min_{\varphi \in [0,\pi]} \Gamma(T,\varphi) \right) = \frac{\Gamma(T,\pi) - \Gamma(T,0)}{\Delta\Gamma_0}. \tag{43}$$

As seen from Fig. 8, this time decay, after a transitional period, is linear in a log-log plot—i.e., it obeys a power law for $T \in [50, 100]$, $\Delta \Gamma_{\rm rel}(T) = \alpha_\Gamma T^{\beta_\Gamma}$. From Fig. 8(b,c), we see that α_Γ and β_Γ depend only weakly on Mg and $\bar{\Gamma}$. The dependence on $\bar{\Gamma}$ is especially weak—the graphs are virtually on top of one another. The dependence on the rescaled bond number is much more substantial, as seen in Fig. 8a. Unfortunately, due to the slow convergence in time, this dependence is difficult to quantify for smaller values of Bo. However, as Bo increases, $\alpha_\Gamma \longrightarrow 0.5$ and $\beta_\Gamma \longrightarrow -0.56$.

The initial surface velocity, $U_s(0, \varphi)$, varies between positive and negative values, in an uneven sinusoidal wave (see Fig. 9). We note that negative surface velocity values indicate an upward surface flow. However, the overall flow is still downward (see Fig. 11). Situations in which the surface flow opposes the overall direction of flow



Page 16 of 28 D. W. Martin, F. Blanchette

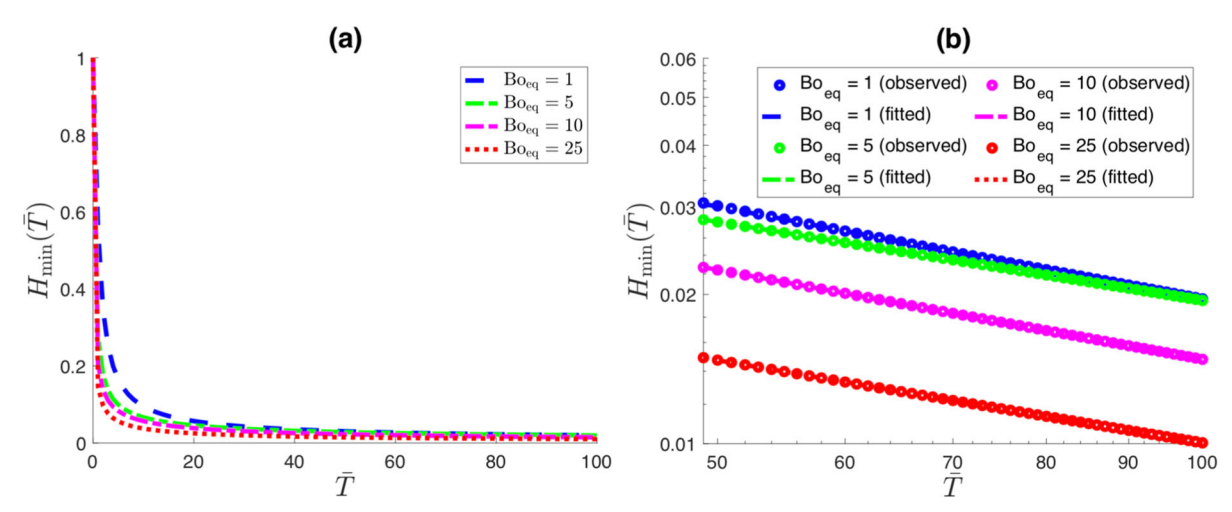


Fig. 6 Time evolution of the minimum half-thickness, H_{\min} , for four different rescaled Bond numbers (a) and long time behavior of the minimum half-thickness, H_{\min} , versus time, both observed and fitted, for four different rescaled Bond numbers (b). The curve fitting is done for times $50 \le \bar{T} \le 100$ and the coefficients are given in Table 6

have been observed before [52]. Smaller Marangoni numbers result in larger initial surface flows, while the initial surface velocity approaches zero as Mg $\longrightarrow \infty$. Similarly, initial surface velocities are zero for Bo = 0 and increase in magnitude with Bo. The initial surface velocity decreases uniformly with increasing average surfactant concentration. This is also unsurprising, as larger values of $\bar{\Gamma}$ result in smaller initial surfactant gradients (see Eq. (42)). These surfactant gradients then decay toward equilibrium more quickly, resulting in larger initial values of $\partial \Gamma/\partial T$ and hence larger initial surface flows.

After a short period of time, the surface velocity becomes strictly negative, which means that surface flow is driven primarily by surfactant gradients, rather than gravity. For long times, the surface velocity decreases to zero, in all cases. The time decay of the surface velocity, $U_s(T,\varphi)$, can be quantified by the time decay of the maximum absolute surface velocity,

$$U_{s,\max}(T) = \max_{\varphi \in [0,\pi]} |U_s(T,\varphi)|.$$

After an initial transition, $U_{s,max}(T)$ is linear in a log-log plot—i.e., it obeys a power law: $U_{s,max}(T) = \alpha_U T^{\beta_U}$ for $T \in [50, 100]$, as shown in Fig. 10.

For Bo = 1, as Mg increases from 2 to 10, α_U decreases from approximately 0.02 to 0.004, while $\beta_U \approx -1.7$ remains approximately constant. As $\bar{\Gamma}$ increases from 0.5 to 0.9, α_U decreases from 0.035 to 0.003, while β_U remains constant at -1.7 to a very good approximation. The dependence of α_U and β_U on Bo is less straightforward, because of the slow convergence in time for small rescaled Bond numbers. However, β_U decreases from -1.46 to -1.55, and α_U more than doubles from 0.005 to 0.011 as the rescaled Bond number increases over the range $6 \le Bo \le 10$. As seen in Fig. 10, the dependence of α_U on Bo, Mg, and $\bar{\Gamma}$ closely mirrors the initial conditions, shown in Fig. 9. In all cases, the behavior of $U_{s,max}(T)$ qualitatively resembles that of $\Delta\Gamma_{rel}(T)$, which supports the claim that surface velocities are driven primarily by surfactant gradients, rather than gravity. Although the surface velocity can be upward, the total flux at any angle φ is always positive (i.e., toward the bottom of the bubble), as shown in Fig. 11. Unsurprisingly, the total flux increases with Bond number (Fig. 11a). Furthermore, the flux decays with time (Fig. 11b).

Although our discussion uses the arbitrarily imposed initial condition, $H(0, \varphi) = 1$, only the initial transition period was found to depend on this initial condition. The results for the long-term time decay are qualitatively similar for any initial condition, as was found when using the initial condition $H(0, \varphi) = 1 - 0.9 \cos \varphi$. Indeed, for $H(0, \varphi) = 1$, $U_{s,max}(T)$ decayed as $U_{s,max}(T) = 0.0036T^{-1.69}$, while for $H(0, \varphi) = 1 - 0.9 \cos \varphi$, it decayed as $U_{s,max}(T) = 0.0021T^{-1.60}$. We mention, also, that due to slow convergence in time, β_U and β_Γ have variations



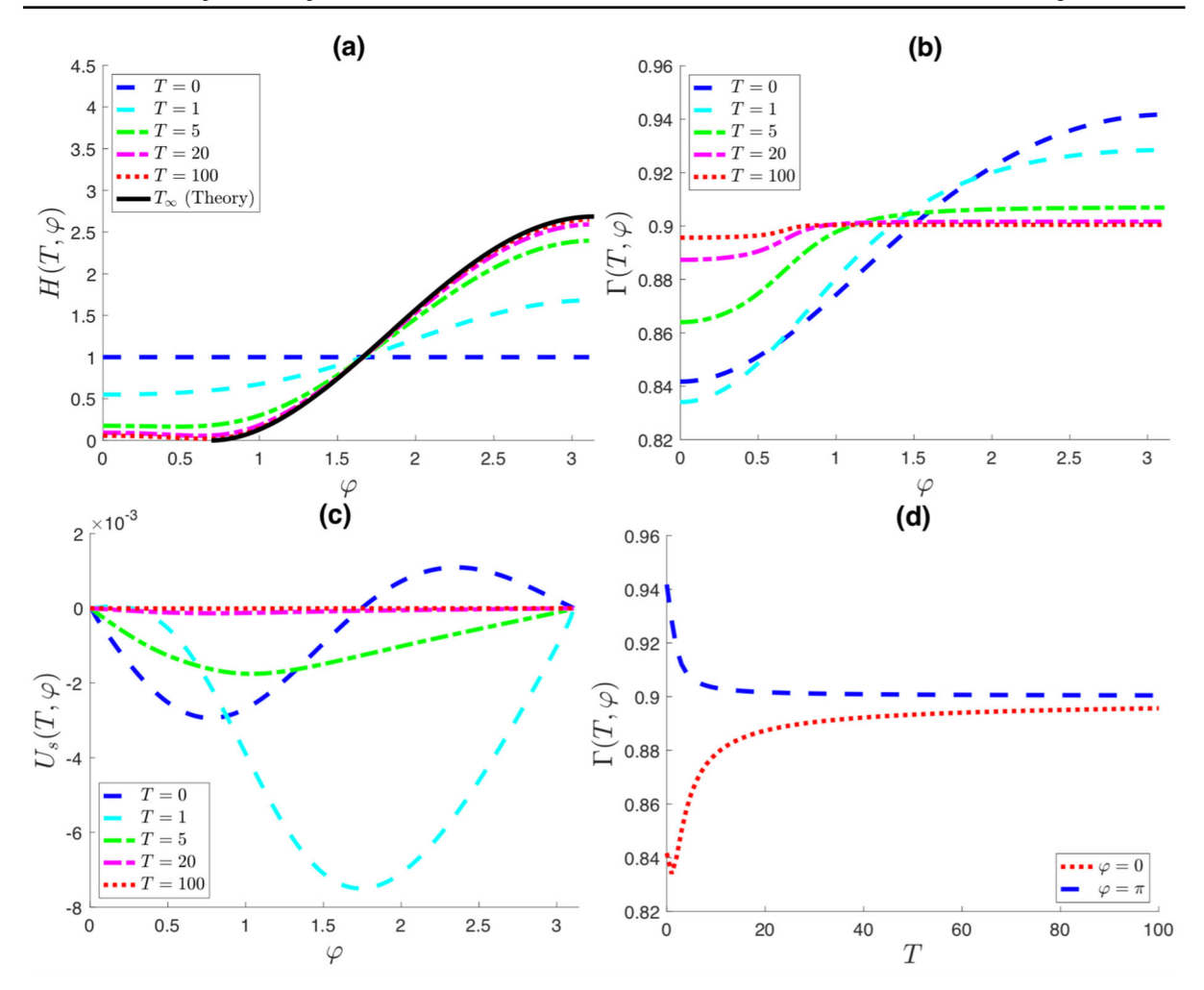


Fig. 7 Film half-thickness (a), surfactant concentration on the surface (b), and surface velocity (c) as a function of the angle from the top, φ , at various times. Panel d shows a time series of surfactant concentration at the top and bottom of the bubble. All panels are computed with Bo = 1, Mg = 2 and $\bar{\Gamma} = 0.9$

on the order of ± 0.1 . Finally, we reiterate that this decay is for intermediate values of time only. In later times, the exponents are likely to change, and disjoining pressure is likely to become a factor.

5 Bubble bursting and minimizing angle

As the film thickness tends to zero, the bubble will eventually burst and we will have $\lim_{T\to\infty} H(T,\varphi_{\rm c})=0$ at some minimizing angle, $\varphi_{\rm c}$. A prediction of this angle follows from Eq. (30). We have observed that the rate of change of the thickness approaches zero as H approaches zero (see Figs. 4 and 5). Furthermore, the power law $H_{\rm min}(T)=\alpha T^{\beta}$ implies $H'_{\rm min}(T)=\mathcal{O}(T^{\beta-1})$, where $-1.5\leq \beta-1\leq -1.6$, so that the time derivative of the minimum thickness decreases to zero for long times. Hence, we consider the approximation that $\partial H/\partial T\approx 0$. Correspondingly, the surface flow also decays in time according to the power law $U_{\rm s,max}(T)=\alpha_U T^{\beta_U}$, so that we may consider the approximation $U_{\rm s}\approx 0$. We have observed from our simulations that drainage eventually divides the interval $0\leq \varphi \leq \pi$ into two regions: one, $\varphi < \varphi_{\rm c}$, in which $H\ll 1$, and one, $\varphi > \varphi_{\rm c}$, in which H is of order



Page 18 of 28 D. W. Martin, F. Blanchette

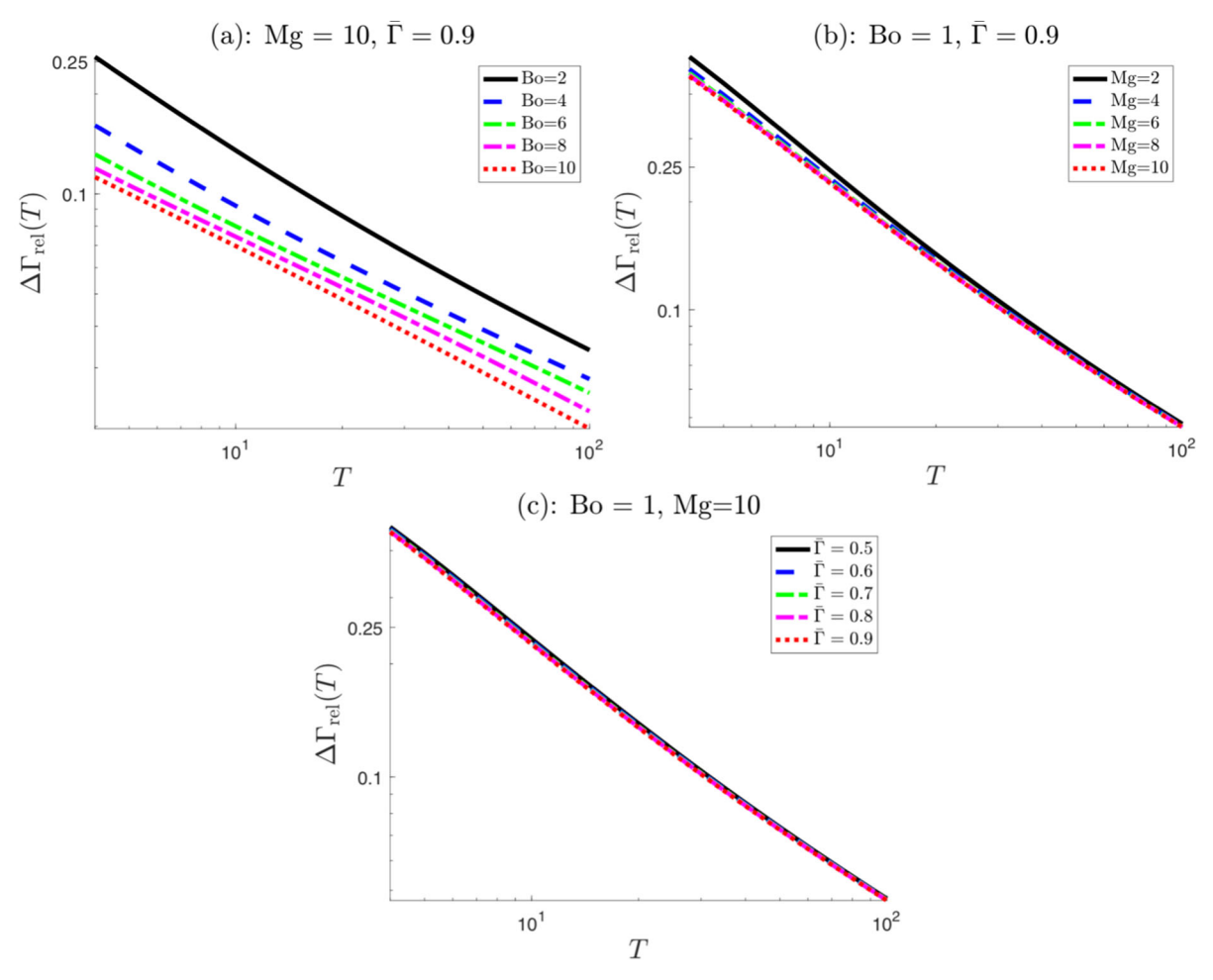


Fig. 8 Time evolution of the relative surfactant difference shown on a logarithmic scale, for different rescaled Bond numbers (a), Marangoni numbers (b), and average surfactant concentrations (c)

one. In the region $\varphi_c \le \varphi \le \pi$, Eq. (30), with the time dependence and surface velocity set to zero, integrates to

$$\frac{\partial}{\partial \varphi} \left(\frac{\partial^2 H}{\partial \varphi^2} + \frac{\partial H}{\partial \varphi} \cot \varphi + 2H \right) = -\text{Bo } \sin \varphi. \tag{44}$$

Eq. (44) then has general solution

$$H_{\infty}(\varphi) \equiv H(\infty, \varphi) = -\frac{1}{6} \left(\cos \varphi \log(1 - \cos \varphi) + \cos \varphi \log(1 + \cos \varphi) \right) \text{Bo}$$

$$+ \tilde{B} \left(\cos \varphi \log(1 - \cos \varphi) - \cos \varphi \log(1 + \cos \varphi) \right) + A \cos \varphi + \tilde{A},$$

$$(45)$$

where \tilde{B} , A, \tilde{A} are constants to be determined by the boundary conditions. We notice that the terms of the form $\cos \varphi \log(1-\cos\varphi)$ become unbounded as $\varphi \longrightarrow 0^+$, and the terms of the form $\cos \varphi \log(1+\cos\varphi)$ become unbounded as $\varphi \longrightarrow \pi^-$. Since both groupings of terms cannot be set to zero simultaneously, it is impossible to obtain a physically feasible solution to the steady-state equation on all of $0 \le \varphi \le \pi$, as was mentioned earlier at the beginning of Sect. 3. However, in the domain $\varphi_c \le \varphi \le \pi$, we only need eliminate the terms of the form $\cos \varphi \log(1+\cos\varphi)$. This can be done by setting $\tilde{B}=-\mathrm{Bo}/6$. We impose the condition that H_∞ be smooth at φ_c , and have a relative minimum. In addition, we impose that at $\varphi = \varphi_c$, the thickness be zero. Altogether,

$$H_{\infty}(\varphi) = -\frac{1}{3}\operatorname{Bo}\cos\varphi\log(1-\cos\varphi) - \frac{1}{3}\operatorname{Bo}\cos\varphi\left(\frac{\cos\varphi_{c}}{1-\cos\varphi_{c}} - \log(1-\cos\varphi_{c})\right) + \frac{1}{3}\operatorname{Bo}\frac{\cos^{2}\varphi_{c}}{1-\cos\varphi_{c}}.$$
 (46)



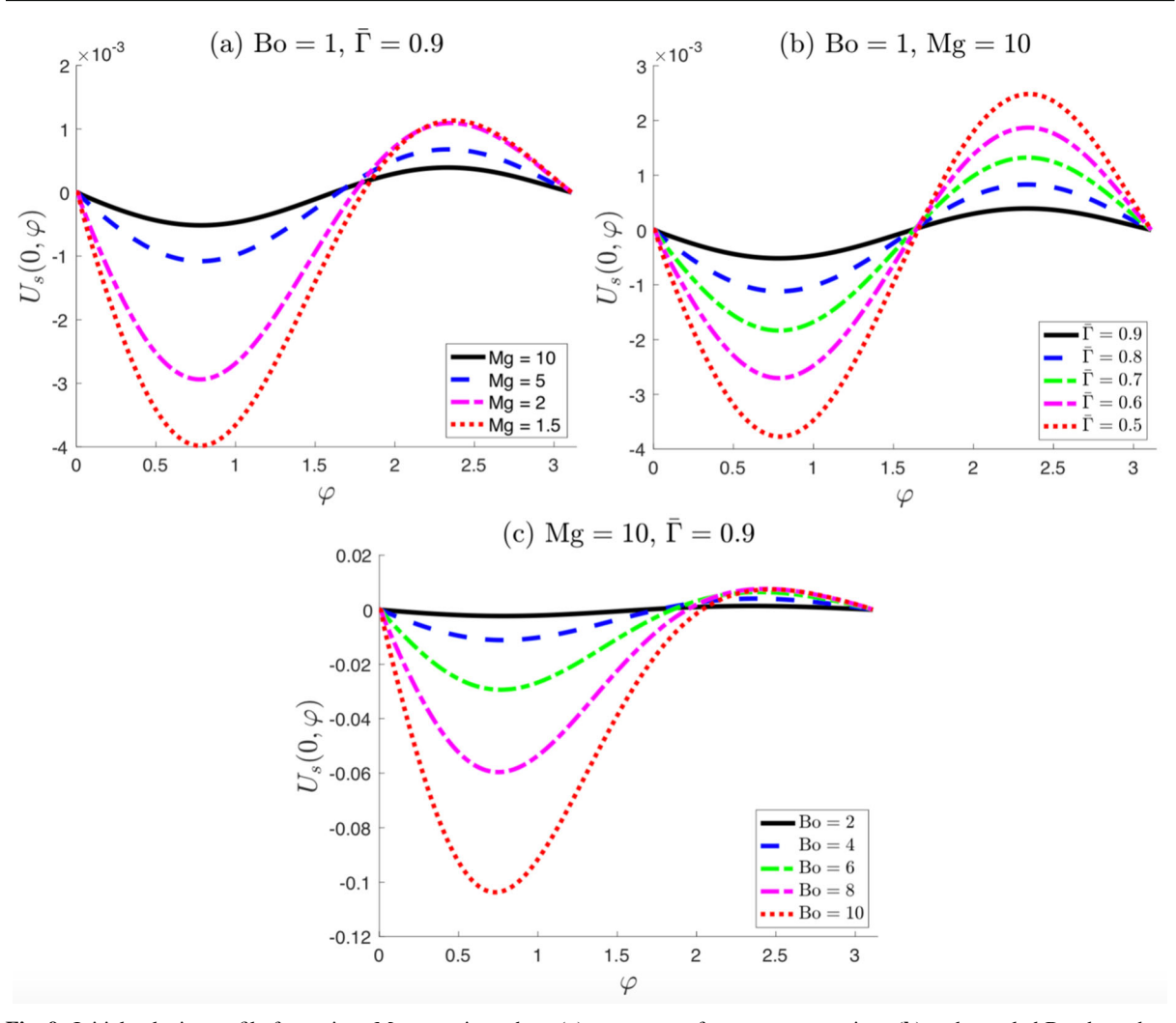


Fig. 9 Initial velocity profile for various Marangoni numbers (a), average surfactant concentrations (b) and rescaled Bond numbers (c), for uniform initial thickness: $H(0, \varphi) = 1$

To determine φ_c , we make use of volume conservation. We do not have a specific way to track the exact fluid volume in the top region ($0 \le \varphi \le \varphi_c$). However, because the film is observed to be very thin in that region, almost all the fluid volume will be located in the region $\varphi_c \le \varphi \le \pi$. Therefore, we make the approximation

$$\int_{\varphi_{\rm c}}^{\pi} H(\infty,\varphi) \, \sin\varphi \, \, \mathrm{d}\varphi \approx \int_{0}^{\pi} H(0,\varphi) \, \sin\varphi \, \, \mathrm{d}\varphi = 2.$$

Although the left-hand side underestimates the fluid volume, we expect that the error will be small as $H(T, \varphi_c)$ approaches zero. Using the form given in Eq. (46) and integrating, we have that the minimizing angle satisfies

$$\frac{24}{\text{Bo}} = \frac{(1 + \cos \varphi_{\text{c}})^3}{1 - \cos \varphi_{\text{c}}}.$$
(47)

We note that Eq. (47) has a single real root that can be obtained analytically which is confined to the interval (-1, 1), and which increases monotonically with Bo (see Appendix D).

We compare this approximate analytical result with numerical simulations of Eq. (33), in which we have recorded the minimum thickness, H_{min} , at T=100 for several rescaled Bond numbers, and the associated minimizing angle, φ_{c} . Figure 12 shows excellent agreement with the predicted values. We note that for Bo = 24, $\varphi_{\text{c}}=\pi/2$, while



Page 20 of 28 D. W. Martin, F. Blanchette

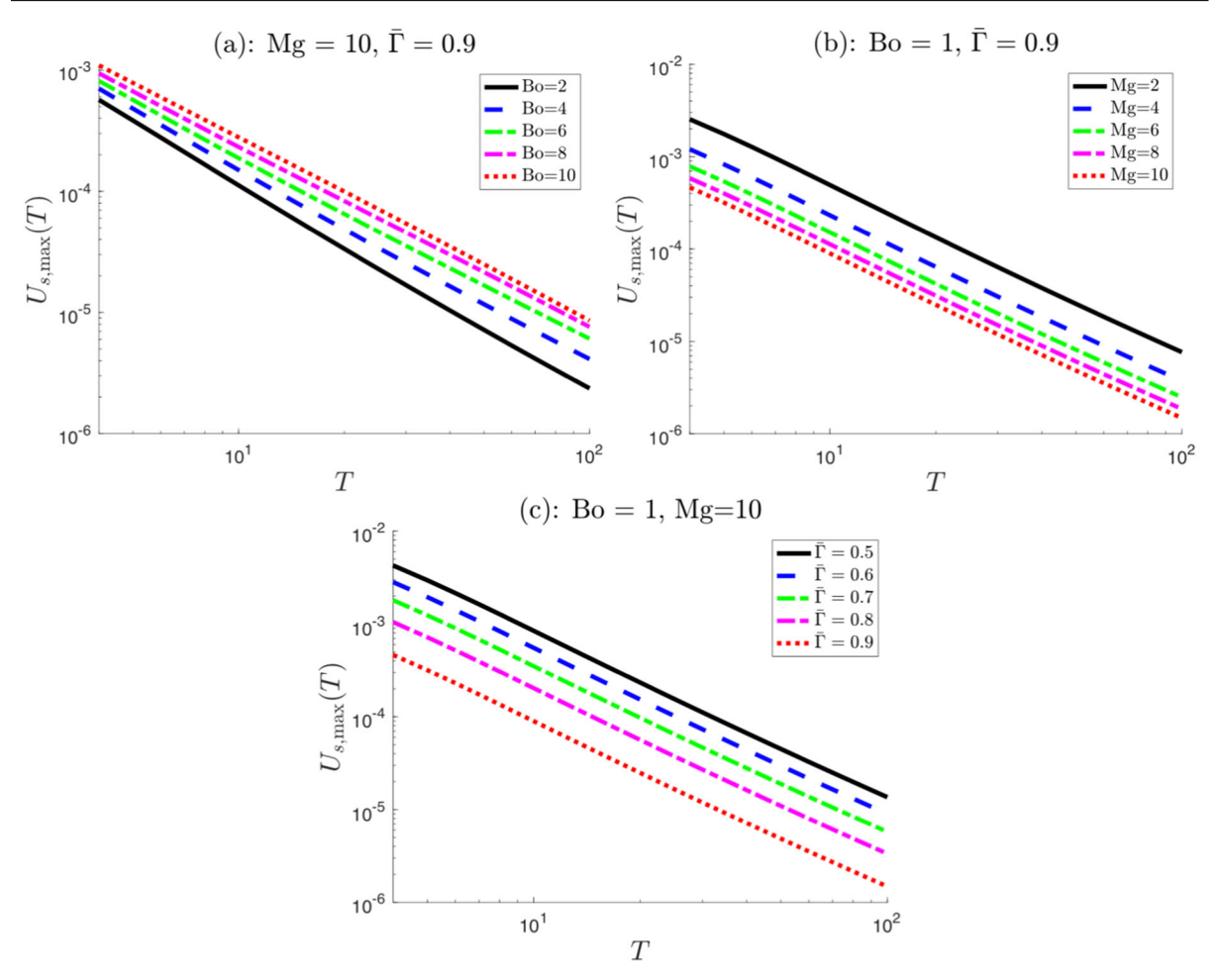


Fig. 10 Time evolution of the maximum absolute surface velocity shown on a logarithmic scale, for different rescaled Bond numbers (a), Marangoni numbers (b), and average surfactant concentrations (c)

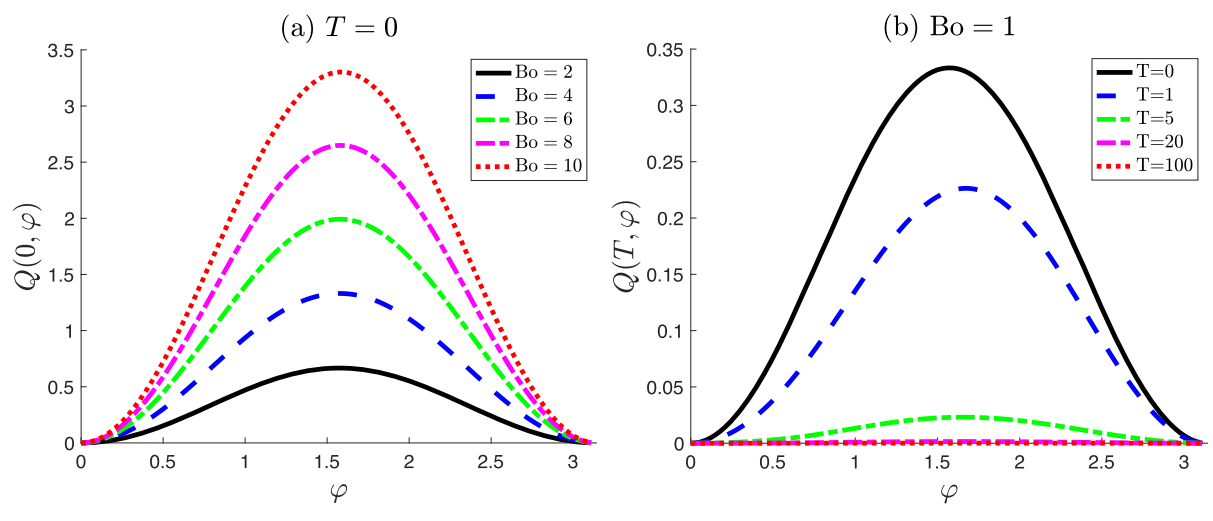


Fig. 11 Initial flux as a function of angle from the top, φ , for various rescaled Bond numbers (a), and flux against φ at various times for Bo = 1 (b). In both cases, Mg = 10 and $\bar{\Gamma} = 0.9$



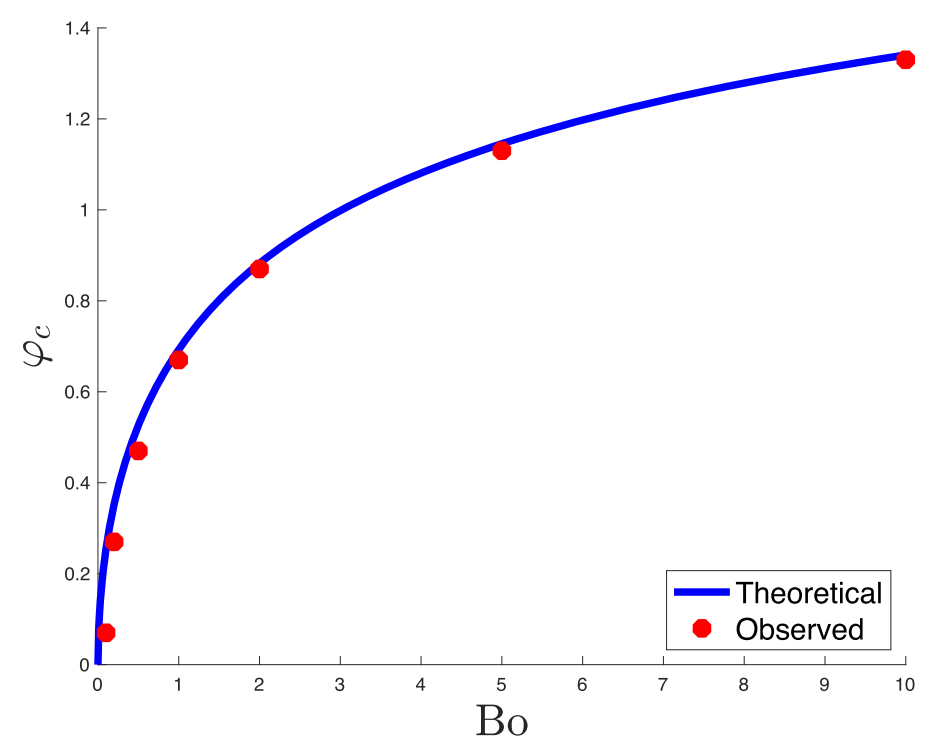


Fig. 12 Minimizing angle, φ_c , at which $H \longrightarrow 0$ first, plotted against the rescaled Bond number. The observed values of φ_c for simulations in which Bo = 0.1, 0.2, 0.5, 1, 2, 5, and 10 are shown as red dots, while the predicted curve based on Eq. (47) is plotted in blue. (Color figure online)

 $\varphi_c \longrightarrow 0$ as Bo $\longrightarrow 0$ and $\varphi_c \longrightarrow \pi$ as Bo $\longrightarrow \infty$. These results are applicable with or without sorption (see Appendix A), and for any value of Mg.

6 Similarity solution

The long-term dynamics of thin films and the approach to their break-up can often be successfully captured by similarity solutions, see e.g., [49–51], including in the presence of Marangoni effects [47]. For long but finite times, our numerical results indicate that the minimum thickness will decay according to a power law. As such, near $\varphi = \varphi_c$ we seek a similarity solution and posit the form

$$H(T, \varphi) = H_{\infty}(\varphi) + T^{\beta} f(\eta) \text{ where } \eta = (\varphi - \varphi_{c})T^{b},$$
 (48)

for $T\gg 1$. Here, $H_\infty(\varphi)$ is given by Eq. (46) for $\varphi>\varphi_{\rm c}$ and $H_\infty(\varphi)=0$ for $\varphi\leq\varphi_{\rm c}$ so that $H_\infty(\varphi)\ll 1$ near $\varphi_{\rm c}$. Because the minimum thickness tends to zero, we assume $\beta<0$. As $T\gg 1$, the size of the region described by the similarity solution shrinks, and so we must have that $b\geq 0$. However, setting b=0 implies that the curvature terms become negligible, which is contradicted by our numerical observations. In particular, the derivative of curvature spikes near $\varphi_{\rm c}$ so that at that location, the curvature and gravity terms remain of comparable magnitude even when Bo $\gg 1$ (see Fig. 13). Hence, we must have b>0. Furthermore, we note that our numerical data indicate that the surface velocity term decays as $U_{\rm s,max}(T)\sim T^{-1.7}$, while $H_{\rm min}(T)\sim T^\beta$ with $-0.6\leq\beta\leq-0.5$. The gravity term therefore decays as $T^{-1.8}$ (or more slowly) and the maximum surface velocity term decays as $T^{-2.2}$ (or faster), rendering it negligible.

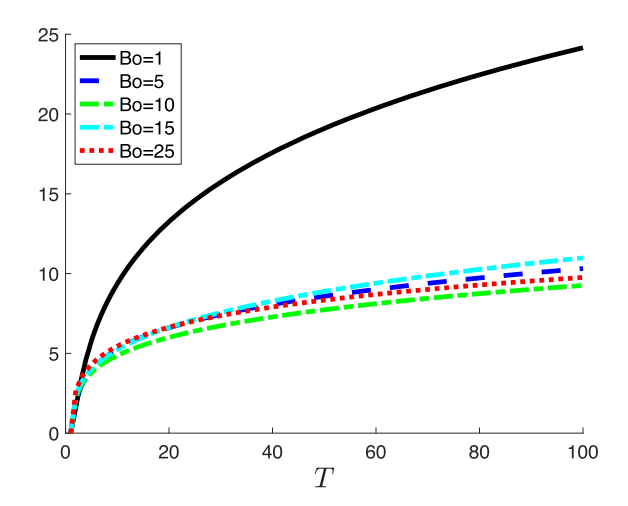
Putting Eq. (48) into Eq. (30) and discarding higher order terms, we obtain

$$\beta T^{-2\beta - 1} f + b\eta T^{-2\beta - 1} f' + f^2 f' \left(T^{\beta + 4b} f''' + T^b \operatorname{Bo} \sin \varphi_{c} \right) + \frac{1}{3} f^3 T^{\beta + 4b} f'''' = 0 \quad \text{for} \quad \varphi < \varphi_{c}$$
 (49)



1 Page 22 of 28 D. W. Martin, F. Blanchette

Fig. 13 Ratio of the curvature to gravity terms appearing in Eq. (33) at the point of minimum thickness, φ_c , over time, for different rescaled Bond numbers. More specifically, the vertical axis is $\frac{1}{\mathrm{Bo}\sin\varphi}\frac{\partial}{\partial\varphi}\left(\frac{\partial^2 H}{\partial\varphi^2}+\frac{\partial H}{\partial\varphi}\cot\varphi+2H\right)\bigg|_{\varphi_c}.$ Here, Mg $\gg 1$



and

$$\beta T^{-2\beta-1} f + b\eta T^{-2\beta-1} f' + f^2 f' T^{\beta+4b} f''' + \frac{1}{3} f^3 T^{\beta+4b} f'''' = 0 \quad \text{for} \quad \varphi > \varphi_c.$$
 (50)

We note that the only difference between Eqs. (49) and (50) is the absence of a gravity term in Eq. (50). This is due to the fact that the curvature of H_{∞} cancels the gravity term, because it is a solution to Eq. (44). Balancing the time dependence in Eq. (50), we obtain $-2\beta - 1 = \beta + 4b$. Balancing the curvature and gravity terms in Eq. (49), we obtain $\beta + 4b = b$, so that $\beta = -3/5$, and b = 1/5. The exponents in Table 6 are close to the value of $\beta = -3/5$, and exactly equal it for Bo = 10 and Bo = 15. It appears that the asymptotic behavior has not quite been reached by the time T = 100.

If we substitute the forms $\Gamma(T, \varphi_c) = \bar{\Gamma} + T^{a_\Gamma} g(\eta)$ and $U_s(T, \varphi_c) = T^{a_U} G(\eta)$ into Eqs. (13) and (31) and discard higher order terms on the assumption that a_Γ , $a_U < 0$ and η is given by Eq. (48), then we obtain $a_\Gamma = -4/5$ and $a_U = -2$. These values indicate significantly faster decay than the observed decay rates for $\Delta \Gamma_{\rm rel}$ and $U_{\rm s,max}$, which is unsurprising, since we expect $\Delta \Gamma_{\rm rel}$ and $U_{\rm s,max}$ to represent the slowest global decay rates of $\Gamma - \bar{\Gamma}$ and $U_{\rm s}$, respectively. The decay rate of Γ and $U_{\rm s}$ is therefore faster at the critical angle than in the rest of the film. This also confirms our assumption that the surface velocity term can be neglected in the similarity solution.

7 Conclusion and discussion

To describe the time evolution of the flow, film thickness, and surfactant concentration of an approximately spherical soap bubble, we have applied lubrication theory to simplify the axisymmetric Stokes, Young–Laplace, Marangoni, and surfactant tracking equations. Integrating across the film surface, we derived a reduced system of equations that capture the most important features of this system.

We studied numerically the transient dynamics for two cases—first, for large Marangoni numbers, in which the tangential flow is suppressed, and second, for a Marangoni number of order 1. In both cases, the minimum film half-thickness approaches zero according to a power law, which is, in dimensional form,

$$h_{\min}(t, \text{Bo}) = h_0 \alpha(\text{Bo}) \left(\frac{t h_0^3 \sigma_0}{\mu r_0^4}\right)^{\beta}, \text{ where } \alpha(\text{Bo}) \in [0.34, 0.13] \text{ and } \beta \in [-0.6, -0.5].$$
 (51)

Although β appears to exhibit a weak time dependence, we have found that for long times, $\beta = -3/5$. Here, Bo is the bond number, representing the relative importance of buoyancy to surface tension, and is assumed to be in the range Bo \in [0, 25]. Although our findings are not directly comparable with any results we are aware of, they are generally consistent with previously published results. In [43], both theoretical and experimental results indicate



where Bo is significantly larger. The simulations presented in [17] Figure 3 show the thickness of the bubble varying by several orders of magnitude, which differs from our observed results for low rescaled Bond number Bo \leq 25, but is consistent with what we would expect for large values of Bo. For example, Eqs. (46) and (47) predict a relative thickness at the bottom of the bubble at long time (quasi steady-state) of $H(\infty, \pi) \approx 77.3$ for Bo = 10^5 , which is consistent with [17] Figure 3. For ordinary soap bubbles, this rescaled Bond number corresponds to a bubble radius of approximately 0.67cm.

Our results for the film evolution may also be compared with experimental results—particularly Figure 3 of [15] and Figure 9 of [16]. In [15], the thickness was observed to vary minimally over time, indicating that the quasi steady-

Our results for the film evolution may also be compared with experimental results—particularly Figure 3 of [15] and Figure 9 of [16]. In [15], the thickness was observed to vary minimally over time, indicating that the quasi steady-state had already been reached, with an exponential model of the form $H(\varphi) = \exp\left(\tilde{a}\cos^2\varphi + \tilde{b}\cos\varphi + \tilde{c}\right)$. In [16], an exponential model of the form $H(\varphi) = \exp\left(\tilde{b}\cos\varphi + \tilde{c}\right)$ was employed, with time-dependent coefficients. In both cases, $\tilde{b} < 0$. When Bo > 1, our results are qualitatively similar to experiments (see Fig. 3), but the regime we focus on is different. Future work may solve the equations we derived in the regime considered in the experiments of [15] and [16] and allow for a more direct comparison, but it is outside the scope of the present work which focuses on a small rescaled Bond number, $1 \le Bo \le 25$.

We also obtained analytical expressions, confirmed by simulations, for the minimizing angle at which the film first tends to zero and where, therefore, the bubble is most likely to burst. However, it is also possible that the bubble bursts away from the exact location of the minimum thickness, given that the thickness varies very slowly near the location of minimum thickness. We are not aware of comparable experimental measurements of the location when bursting is initiated, despite the importance of this feature on the dispersion of the droplets generated by bursting [6–9,53].

Our derivation of general lubrication equations describing the dynamics of spherical films opens the door to several other possible avenues for future research. Evaporative effects eventually become important. These may be included in future work by considering a slowly varying film thickness h_0 and corresponding changes in bulk and surface surfactant concentrations which would allow a more complete picture of the lifespan of a soap bubble. Another research area left to explore is the stability of soap bubbles to non-axisymmetric perturbations. While experimental results, e.g., [15,16], confirm that the axisymmetric solutions are indeed realized, casual observations of soap bubbles and recent simulations [18] show that they are sensitive to symmetry-breaking perturbations. Though Marangoni effects are stabilizing against thickness perturbations, they may create oscillatory responses to surfactant concentration imperfections [43,54].

Finally, we note that our results give a good description of fully spherical bubbles, an idealized set-up corresponding to bubbles tethered at the bottom or resting on a hydrophobic surface. More generally, soap bubbles may be deformed by gravitational effects or external forcing. The general trends found to dominate here should also be dominant for deformed bubbles, but a more detailed treatment of the effects of shape deformations remains to be undertaken. Moreover, commonly encountered soap bubbles are shaped as spherical caps that rest on a liquid surface or substrate. The equations derived here may be applied to such bubbles, though they will need to be supplemented by appropriate boundary conditions [42,55,56].

Appendix A: Soluble surfactant

The surfactant concentration in the film, c, (in mass per volume) satisfies an advection-diffusion equation, given, in dimensional form, as

$$\frac{\partial c}{\partial t} + \bar{\nabla} \cdot (\mathbf{u}c) = k_{\rm c} \bar{\nabla}^2 c,\tag{52}$$



1 Page 24 of 28 D. W. Martin, F. Blanchette

where k_c is the bulk diffusivity and $\bar{\nabla}$ is a dimensional gradient. In the presence of sorption, Eq. (4) is supplemented with a bulk exchange term [37,38],

$$\frac{\partial \gamma}{\partial t} + \bar{\nabla}_{s} \cdot (\mathbf{u}_{s}\gamma) = k_{\Gamma} \bar{\nabla}_{s}^{2} \gamma + j(\gamma, c_{s}), \tag{53}$$

where k_{Γ} is a diffusivity of surface surfactant. Combining Eq. (52) with the exchange term, we obtain a boundary condition on the bulk concentration,

$$j(\gamma, c_{\rm S}) = -k_{\rm c}(\mathbf{n} \cdot \bar{\nabla})c_{\rm S},\tag{54}$$

where \mathbf{n} is the outward unit normal at h. To describe the bulk exchange term, we can apply the constitutive relation [37,38]

$$-j(\gamma, c_{\rm s}) = k_{\rm ad}c_{\rm s} \left(1 - \frac{\gamma}{\gamma_{\infty}}\right) - k_{\rm de}\gamma,\tag{55}$$

where $k_{\rm ad}$ and $k_{\rm de}$ are kinetic constants of adsorption and desorption, with units of m/s and s⁻¹, respectively.

To obtain dimensionless equations, we define $C = c/c_0$ where c_0 is the equilibrium bulk concentration. The exchange term in Eq. (55) rescales to $J(\Gamma, C_s) = j(\gamma, C_s)/(\gamma_{\infty}u_0/r_0)$. To describe it more precisely, we write the gradient of the bulk concentration in coordinates, (φ, R) :

$$\bar{\nabla}c = \left(\frac{1}{r}\frac{\partial c}{\partial \varphi}, \frac{\partial c}{\partial r}\right) = \frac{c_0}{r_0} \left(\frac{\partial C}{\partial \varphi}, \frac{1}{\varepsilon}\frac{\partial C}{\partial R}\right),$$

so that in rescaled coordinate form, Eq. (54) becomes, on the outer film,

$$-J(\Gamma, C_{\rm s}) = \frac{1}{L \operatorname{Pe}_{\rm c}} \left(\frac{\partial C}{\partial R} \Big|_{\rm s} - \varepsilon^2 \frac{\partial H}{\partial \varphi} \frac{\partial C}{\partial \varphi} \Big|_{\rm s} \right) \left(1 + \varepsilon^2 \left(\frac{\partial H}{\partial \varphi} \right)^2 \right)^{-1/2} = \frac{1}{L \operatorname{Pe}_{\rm c}} \frac{\partial C}{\partial R} \Big|_{\rm s} + \mathcal{O}(\varepsilon), \tag{56}$$

where L is a dimensionless surfactant depletion length $L = \gamma_{\infty}/h_0c_0$. The expression on the inner film is the same but with the opposite sign of the R derivative. Rescaling, we obtain

$$J(\Gamma, C_s) = -\text{Bi}(\text{Ad}C_s(1-\Gamma) - \Gamma), \tag{57}$$

where we have introduced a Biot number and an adsorption number

Bi =
$$\frac{r_0 k_{\text{de}}}{u_0}$$
 and Ad = $\frac{k_{\text{ad}} c_0}{k_{\text{de}} \gamma_{\infty}}$.

Then, if we discard higher order terms, Eqs. (52) and (53) rescale to

$$\frac{\partial C}{\partial T} + \frac{\partial}{\partial R} (VC) + \frac{1}{\sin \varphi} \frac{\partial}{\partial \varphi} (UC \sin \varphi) = \frac{1}{\text{Pe}_c} \frac{\partial^2 C}{\partial R^2},$$
(58)

and

$$\frac{\partial \Gamma}{\partial T} + \frac{1}{\sin \varphi} \frac{\partial}{\partial \varphi} (U_{\rm S} \Gamma \sin \varphi) = \frac{1}{\text{Pe}_{\Gamma} \sin \varphi} \frac{\partial}{\partial \varphi} \left(\sin \varphi \frac{\partial \Gamma}{\partial \varphi} \right) + J(\Gamma, C_{\rm S}), \tag{59}$$

where

$$Pe_{c} = \frac{\varepsilon^{2} r_{0} u_{0}}{k_{c}} \quad \text{and} \quad Pe_{\Gamma} = \frac{r_{0} u_{0}}{k_{\Gamma}}, \tag{60}$$

are Péclet numbers associated to the bulk and to the surface, respectively. Note that the factor of ε^2 in Pe_c ensures that Pe_c is likely much smaller than Pe_{\Gamma}. In general, surface diffusion, i.e., $1/\text{Pe}_{\Gamma}$, tends to be very small. The symmetry of the system results in the condition $\frac{\partial C}{\partial R}\big|_{R=0} = 0$ at the center of the film.

Proceeding in a manner similar to Sect. 2.5, we integrate the bulk surfactant equation, Eq. (58), across the film, using Eq. (17) and the boundary conditions (21) and (56). We obtain

$$\frac{\partial}{\partial T} \int_0^H C \, \mathrm{d}R + \frac{1}{\sin \varphi} \frac{\partial}{\partial \varphi} \left(\sin \varphi \int_0^H U C \, \mathrm{d}R \right) = -LJ(\Gamma, C_\mathrm{s}). \tag{61}$$



Here, we derive equations (19) and (20) from Eq. (16). In axisymmetric spherical coordinates, the components of the stress tensor are given by

$$\tau_{rr} = -p + 2\mu \frac{\partial v}{\partial r},\tag{62}$$

$$\tau_{\varphi\varphi} = -p + 2\mu \left(\frac{1}{r} \frac{\partial u}{\partial \varphi} + \frac{v}{r} \right) \text{ and}$$
(63)

$$\tau_{r\varphi} = \mu \left(\frac{1}{r} \frac{\partial v}{\partial \varphi} + \frac{\partial u}{\partial r} - \frac{v}{r} \right). \tag{64}$$

In dimensionless form, the components of the stress tensor rescale as

$$T_{rr} = -P + \mathcal{O}(\varepsilon^2),\tag{65}$$

$$T_{\varphi\varphi} = -P + \mathcal{O}(\varepsilon^2)$$
 and (66)

$$T_{r\varphi} = \varepsilon \frac{\partial U}{\partial R} + \mathcal{O}(\varepsilon^2). \tag{67}$$

Now we write the outward unit normal, **n**, and the unit tangent, **t**, in terms of $\mathbf{r} = r(\sin\varphi\cos\theta, \sin\varphi\sin\theta, \cos\varphi)$,

$$\mathbf{t} = \left\| \frac{\partial \mathbf{r}}{\partial \varphi} \right\|^{-1} \frac{\partial \mathbf{r}}{\partial \varphi} = \frac{\frac{\partial r}{\partial \varphi} \hat{\mathbf{r}} + r \hat{\boldsymbol{\varphi}}}{\sqrt{\left(\frac{\partial r}{\partial \varphi}\right)^2 + r^2}} = \varepsilon \frac{\partial H}{\partial \varphi} \hat{\mathbf{r}} + \hat{\boldsymbol{\varphi}} + \mathcal{O}(\varepsilon^2), \tag{68}$$

and
$$\mathbf{n} = \left\| \frac{\partial \mathbf{r}}{\partial \varphi} \times \frac{\partial \mathbf{r}}{\partial \theta} \right\|^{-1} \frac{\partial \mathbf{r}}{\partial \varphi} \times \frac{\partial \mathbf{r}}{\partial \theta} = \frac{-\frac{\partial \mathbf{r}}{\partial \varphi} \hat{\boldsymbol{\varphi}} + r \hat{\mathbf{r}}}{\sqrt{\left(\frac{\partial r}{\partial \varphi}\right)^2 + r^2}} = \hat{\mathbf{r}} - \varepsilon \frac{\partial H}{\partial \varphi} \hat{\boldsymbol{\varphi}} + \mathcal{O}(\varepsilon^2),$$
 (69)

where $\hat{\mathbf{r}}$ is the unit vector in the radial direction and $\hat{\boldsymbol{\varphi}}$ is the unit vector in the angular direction. Now, we calculate the total curvature (the sum of the two principal curvatures), following [57]

$$\kappa = \frac{\det\left(\frac{\partial^{2}\mathbf{r}}{\partial\varphi^{2}}\frac{\partial\mathbf{r}}{\partial\varphi}\frac{\partial\mathbf{r}}{\partial\theta}\right)\left|\frac{\partial\mathbf{r}}{\partial\theta}\right|^{2} - 2\det\left(\frac{\partial^{2}\mathbf{r}}{\partial\varphi\partial\theta}\frac{\partial\mathbf{r}}{\partial\varphi}\frac{\partial\mathbf{r}}{\partial\theta}\right)\left(\frac{\partial\mathbf{r}}{\partial\varphi}\cdot\frac{\partial\mathbf{r}}{\partial\theta}\right) + \det\left(\frac{\partial^{2}\mathbf{r}}{\partial\theta^{2}}\frac{\partial\mathbf{r}}{\partial\varphi}\frac{\partial\mathbf{r}}{\partial\theta}\right)\left|\frac{\partial\mathbf{r}}{\partial\varphi}\right|^{2}}{\left(\left|\frac{\partial\mathbf{r}}{\partial\varphi}\right|^{2}\left|\frac{\partial\mathbf{r}}{\partial\theta}\right|^{2} - \left(\frac{\partial\mathbf{r}}{\partial\varphi}\cdot\frac{\partial\mathbf{r}}{\partial\theta}\right)^{2}\right)^{3/2}} \quad .$$
(70)

We obtain

$$K = r_0 \kappa = -2 + \varepsilon \left(\frac{\partial^2 H}{\partial \varphi^2} + \frac{\partial H}{\partial \varphi} \cot \varphi + 2H \right) + \mathcal{O}(\varepsilon^2). \tag{71}$$

Next, we write Eq. (16) explicitly in normal and tangential components, using Eqs. (68) and (69), and keeping in mind the form of the Cauchy stress tensor,

$$\mathbf{T} = T_{rr}\hat{\mathbf{r}} \otimes \hat{\mathbf{r}} + T_{r\omega}\hat{\mathbf{r}} \otimes \hat{\boldsymbol{\varphi}} + T_{\omega r}\hat{\boldsymbol{\varphi}} \otimes \hat{\mathbf{r}} + T_{\omega\omega}\hat{\boldsymbol{\varphi}} \otimes \hat{\boldsymbol{\varphi}}$$

to obtain

$$\mathbf{n} \cdot \mathbf{T} \cdot \mathbf{n} = \left(\varepsilon^2 \left(\frac{\partial H}{\partial \varphi} \right)^2 T_{\varphi \varphi} - 2\varepsilon \frac{\partial H}{\partial \varphi} T_{r\varphi} + T_{rr} \right) / \left(1 + \varepsilon^2 \left(\frac{\partial H}{\partial \varphi} \right)^2 \right) = \Sigma \frac{\partial^2 H}{\partial \varphi^2} + \mathcal{O}(\varepsilon) \text{ and}$$

$$\mathbf{t} \cdot \mathbf{T} \cdot \mathbf{n} = \left(\varepsilon \frac{\partial H}{\partial \varphi} (T_{rr} - T_{\varphi \varphi}) + T_{r\varphi} \left(1 - \varepsilon^2 \left(\frac{\partial H}{\partial \varphi} \right)^2 \right) \right) / \left(1 + \varepsilon^2 \left(\frac{\partial H}{\partial \varphi} \right)^2 \right) = \frac{1}{\varepsilon} \frac{\partial \Sigma}{\partial \varphi} + \mathcal{O}(\varepsilon).$$

Substituting in Eqs. (65) and (67) and taking leading order terms, we obtain Eqs. (19) and (20).



1 Page 26 of 28 D. W. Martin, F. Blanchette

Appendix C: Analysis of the large Marangoni number limit

For El = $\mathcal{O}(1)$ and Mg = $\mathcal{O}(\varepsilon^{-2}) \gg 1$, we expand Γ , U_s , and H in powers of Mg⁻¹,

$$\Gamma(T, \varphi, \mathrm{Mg}) = \Gamma_{(0)}(T, \varphi) + \mathrm{Mg}^{-1}\Gamma_{(1)}(T, \varphi) + \mathcal{O}(\mathrm{Mg}^{-2}),$$

$$U_{s}(T, \varphi, Mg) = U_{s(0)}(T, \varphi) + Mg^{-1}U_{s(1)}(T, \varphi) + \mathcal{O}(Mg^{-2}), \tag{72}$$

and
$$H(T, \varphi, Mg) = H_{(0)}(T, \varphi) + Mg^{-1}H_{(1)}(T, \varphi) + \mathcal{O}(Mg^{-2}).$$

Substituting this result into Eq. (28) and Taylor expanding the logarithm, we obtain

$$\left. \mathrm{Mg}^{-1} \frac{\partial U}{\partial R} \right|_{R=H} = \frac{\partial}{\partial \varphi} \left(\log(1 - \Gamma_{(0)}) - \mathrm{Mg}^{-1} \frac{\Gamma_{(1)}}{1 - \Gamma_{(0)}} \right) + \mathcal{O}(\mathrm{Mg}^{-2}). \tag{73}$$

The leading order term in this equation implies that $\Gamma_{(0)}$ is independent of φ . In fact, surfactant conservation, combined with our assumption of insolubility, additionally implies that $\Gamma_{(0)}$ is constant in time, so $\Gamma_{(0)} = \bar{\Gamma}$, where $\bar{\Gamma}$ is the average surfactant concentration on the film.

The $\mathcal{O}(Mg^{-1})$ terms in Eq. (73) can be substituted into the radial derivative of Eq. (25), to obtain

$$\frac{1}{1-\bar{\Gamma}}\frac{\partial\Gamma_1}{\partial\varphi} = H_{(0)}\left(\frac{\partial P}{\partial\varphi} - \operatorname{Bo}\sin\varphi\right). \tag{74}$$

Substituting Eq. (72) into Eq. (14), we find that

$$\Sigma = 1 + \text{El}\log(1 - \bar{\Gamma}) + \frac{\text{El}\Gamma_1(T, \varphi)}{\text{Mg}(1 - \bar{\Gamma})} + \mathcal{O}(\text{Mg}^{-2}) = \Sigma_{\text{eq}} + \mathcal{O}(\text{Mg}^{-1})$$

where $\Sigma_{eq} = 1 + \text{El} \log(1 - \bar{\Gamma})$ is the equilibrium surface tension of the film. Thus, we can substitute Eq. (19) into Eq. (74), to find

$$\frac{\partial \Gamma_{(1)}}{\partial \varphi} = -(1 - \bar{\Gamma})H_{(0)} \left(\sum_{eq} \frac{\partial}{\partial \varphi} \left(\frac{\partial^2 H_{(0)}}{\partial \varphi^2} + \frac{\partial H_{(0)}}{\partial \varphi} \cot \varphi + 2H_{(0)} \right) + \operatorname{Bo} \sin \varphi \right). \tag{75}$$

Then, the $\mathcal{O}(Mg^{-1})$ terms yield the equation

$$\frac{\partial \Gamma_{(1)}}{\partial T} + \frac{\Gamma_{(0)}}{\sin \varphi} \frac{\partial}{\partial \varphi} (U_{s(1)} \sin \varphi) = 0. \tag{76}$$

By defining a new rescaled Bond number, Bo_{eq} (32) in terms of the equilibrium surface tension $\Sigma_{\rm eq}$ rather than the surfactant-free surface tension, and a new timescale, \bar{T} , based on the equilibrium surface tension, we obtain an equation similar to Eq. (30). Substituting Eq. (72) into Eq. (13), and taking the leading order terms only, we obtain $U_{\rm s(0)} = 0$. Dropping the subscript (0) in $H_{(0)}$, we have (33). Finally, although our analysis assumes Mg = $\mathcal{O}(\varepsilon^{-2})$, our numerical results indicate that $U_{\rm s}$ is negligible even for moderate values of Mg (see Fig. 10).

Appendix D: Exact root of Eq. (47)

If we define $\xi = 1 + \cos \varphi_c$, then Eq. (47) takes the form

$$\frac{24}{\text{Bo}} = \frac{\xi^3}{2 - \xi}$$
 or $\xi^3 + \frac{24}{\text{Bo}}\xi - \frac{48}{\text{Bo}} = 0$.

This is a depressed cubic with coefficients 24/Bo and -48/Bo. The discriminant of the equation is then

$$\Delta = -4 \left(\frac{24}{\text{Bo}}\right)^2 \left(27 + \frac{96}{\text{Bo}}\right).$$

For Bo > 0, this discriminant is always negative, guaranteeing a single real root. That root then yields

$$\cos \varphi_{c} = \left(\frac{24}{Bo}\right)^{1/3} \left(\left(\sqrt{1 + \frac{8}{9Bo}} + 1\right)^{1/3} - \left(\sqrt{1 + \frac{8}{9Bo}} - 1\right)^{1/3} \right) - 1 \tag{77}$$

Note that this is confined to the interval (-1, 1), and is monotonic.



References

- Sha Y, Li Z, Wang Y (2011) The Marangoni convection induced by acetone desorption from the falling soap film. Heat and Mass Transf 48(5):749
- 2. Stefanus S, Steers S, Goldburg WI (2011) Direct measurement of turbulent shear. Physica D 240(23):1873–1876
- 3. Kostarev K, Viviani A, Zuev A (2006) Thermal and concentrational Marangoni convection at liquid/air bubble interface. J Appl Mech 73:66
- 4. Van Nierop EA, Scheid B, Stone HA (2008) On the thickness of soap films: an alternative to Frankel's law. J Fluid Mech 602:119–127
- 5. Karakashev SI (2017) Hydrodynamics of foams. Exp Fluids 58:91
- 6. Bremond N, Villermaux E (2005) Bursting thin liquid films. J Fluid Mech 524:121-130
- 7. Lhuissier H, Villermaux E (2009) Soap films burst like flapping flags. Phys Rev Lett 103:054501
- 8. Müller F, Bohley C, Stannarius R (2009) Second sound in bursting freely suspended smectic-A films. Phys Rev E 79:046315
- 9. Müller F, Stannarius R (2009) Comparison of the rupture dynamics of smectic bubbles and soap bubbles. Liq Cryst 36(2):133–145
- Couder Y, Basdevant C (1986) Experimental and numerical study of vortex couples in two-dimensional flows. J Fluid Mech 173:225–251
- 11. Kellay H, Wu XL, Goldberg WI (1998) Vorticity measurements in turbulent soap films. Phys Rev Lett 80:277-280
- 12. Belmonte A, Goldberg WI, Kellay H, Rutgers MA, Martin B, Wu XL (1999) Velocity fluctuations in a turbulent soap film: the third moment in two dimensions. Phys Fluids 11:1196–1200
- 13. Kellay H, Goldburg WI (2002) Two-dimensional turbulence: a review of some recent experiments. Rep Prog Phys 65(5):845
- 14. Vorobieff P, Rivera M, Ecke RE (1999) Soap film flows: statistics of two-dimensional turbulence. Phys Fluids 11(8):2167-2177
- 15. Lv W, Zhou H, Lou C, Zhu J (2012) Spatial and temporal film thickness measurement of a soap bubble based on large lateral shearing displacement interferometry. Appl Opt 51(36):8863–8872
- Lv W, Zhou H, Zhu J (2012) Thickness measurement of full field soap bubble film in real time based on large lateral shearing displacement interferometry. AIP Conf Proc 1428(1):209–216
- 17. Vitry Y, Dorbolo S, Vermant J, Scheid B (2019) Controlling the lifetime of antibubbles. Adv Coll Interface Sci 270:73–86
- 18. Huang W, Iseringhausen J, Kneiphof T, Qu Z, Jiang C, Hullin MB (2020) Chemomechanical simulation of soap film flow on spherical bubbles. ACM Trans Graph 39(41):1–13
- 19. Ishida S, Synak P, Narita F, Hachisuka T, Wojtan C (2020) A model for soap film dynamics with evolving thickness. ACM Trans Graph 39(31):1–11
- 20. Reynolds O (1886) I. On the theory of lubrication and its application to Mr. Beauchamp Tower's experiments, including an experimental determination of the viscosity of olive oil. Proc R Soc Lond 40(242–245):191–203
- 21. Oron A, Davis SH, Bankoff SG (1997) Long-scale evolution of thin liquid films. Rev Mod Phys 69:931-980
- 22. Jain RK, Ruckenstein E (1976) Stability of stagnant viscous films on a solid surface. J Colloid Interface Sci 54(1):108-116
- 23. Sharma A, Ruckenstein E (1986) An analytical nonlinear theory of thin film rupture and its application to wetting films. J Colloid Interface Sci 113(2):456–479
- 24. Oron A, Rosenau P (1989) Nonlinear evolution and breaking of interfacial Rayleigh-Taylor waves. Phys Fluids A 1(7):1155-1165
- 25. Burelbach JP, Bankoff SG, Davis SH (1988) Nonlinear stability of evaporating/condensing liquid films. J Fluid Mech 195:463–494
- 26. Erneux T, Davis SH (1993) Nonlinear rupture of free films. Phys Fluids A 5(5):1117–1122
- 27. Davis SH (1987) Thermocapillary instabilities. Annu Rev Fluid Mech 19(1):403-435
- 28. Reisfeld B, Bankoff SG (1990) Nonlinear stability of a heated thin liquid film with variable viscosity. Phys Fluids A 2(11):2066–2067
- 29. Jensen OE, Grotberg JB (1993) The spreading of heat or soluble surfactant along a thin liquid film. Phys Fluids A 5(1):58-68
- 30. De Wit A, Gallez D, Christov CI (1994) Nonlinear evolution equations for thin liquid films with insoluble surfactants. Phys Fluids 6(10):3256–3266
- 31. Yarin AL, Oron A, Rosenau P (1993) Capillary instability of thin liquid film on a cylinder. Phys Fluids A 5(1):91–98
- 32. Reisfeld B, Bankoff SG (1992) Non-isothermal flow of a liquid film on a horizontal cylinder. J Fluid Mech 236:167-196
- 33. Takagi D, Huppert HE (2010) Flow and instability of thin films on a cylinder and sphere. J Fluid Mech 647:221–238
- 34. Blawzdziewicz J, Wajnryb E, Loewenberg M (1999) Hydrodynamic interactions and collision efficiencies of spherical drops covered with an incompressible surfactant film. J Fluid Mech 395:29–59
- 35. Sett S, Sinha-Ray S, Yarin AL (2013) Gravitational drainage of foam films. Langmuir 29(16):4934-4947
- Leal LG (2007) Advanced transport phenomena: fluid mechanics and convective transport processes. Cambridge University Press, New York
- 37. Chang CH, Franses EI (1992) Modified Langmuir-Hinselwood kinetics for dynamic adsorption of surfactants at the air/water interface. Colloids Surf 69(2–3):189–201
- 38. Eggleton CD, Stebe KJ (1998) An adsorption-desorption-controlled surfactant on a deforming droplet. J Colloid Interface Sci 208:68–80
- Cristini V, Blawzdziewicz J, Loewenberg M (1998) Near-contact motion of surfactant-covered spherical drops. J Fluid Mech 366:259–287
- Lyu S (2003) Block copolymers suppressing droplet coalescence through stopping film rupture. Macromolecules 36(26):10052– 10055



1 Page 28 of 28 D. W. Martin, F. Blanchette

41. Vannozzi C (2012) Coalescence of surfactant covered drops in extensional flows: Effects of the interfacial diffusivity. Phys Fluids 24:08

- 42. Cohen C, Darbois Texier B, Reyssat E, Snoeijer JH, Quéré D, Clanet C (2017) On the shape of giant soap bubbles. Proc Natl Acad Sci 114(10):2515–2519
- 43. Sett S, Sahu RP, Sinha-Ray S, Yarin AL (2014) Superspreaders versus "cousin" non-superspreaders: disjoining pressure in gravitational film drainage. Langmuir 30(10):2619–2631
- 44. De Gennes PG, Brochard-Wyart F, Quéré D (2002) Gouttes, bulles perles et ondes. Belin, Paris
- 45. Ungarish M (2009) An introduction to gravity currents and intrusions. CRC Press, Boca Raton
- 46. Singh G, Hirasaki GJ, Miller CA (1996) Effect of material properties on the drainage of symmetric, plane parallel, mobile foam films. J Colloid Interface Sci 184:92–105
- Yeo LY, Matar OK, Perez ES, Hewitt GF (2001) The dynamics of Marangoni-driven local film drainage between two drops. J Colloid Interface Sci 241(1):233–247
- 48. Bergeron V (1999) Forces and structure in thin liquid soap films. J Phys: Condens Matter 11(19):R215–R238
- Constantin P, Dupont TF, Goldstein RE, Kadanoff LP, Shelley MJ, Zhou SM (1993) Droplet breakup in a model of the Hele-Shaw cell. Phys Rev E 47(6):4169–4181
- Bertozzi AL, Brenner MP, Dupont TF, Kadanoff LP (1994) Singularities and similarities in interface flows. Springer, New York, pp 155–208
- 51. Eggers J (1997) Nonlinear dynamics and breakup of free-surface flows. Rev Mod Phys 69:865–930
- 52. Vitasari D, Grassia P, Martin P (2015) Surfactant transport onto a foam film in the presence of surface viscous stress. Appl Math Model 40:10
- 53. Bhakta A, Ruckenstein E (1997) Decay of standing foams: drainage, coalescence and collapse. Adv Colloid Interface Sci 70:1–124
- 54. Burgess JM, Bizon C, McCormick WD, Swift JB, Swinney HL (1999) Instability of the Kolmogorov flow in a soap film. Phys Rev E 60(1):715–21
- 55. Wegener PP, Parlange JY (1973) Spherical-cap bubbles. Annu Rev Fluid Mech 5(1):79–100
- 56. Byakova AV, Gnyloskurenko SV, Nakamura T, Raychenko OI (2003) Influence of wetting conditions on bubble formation at orifice in an inviscid liquid: Mechanism of bubble evolution. Colloids Surf A 229(1–3):19–32
- 57. Abbena E, Salamon S, Gray A (2006) Modern differential geometry of curves and surfaces with mathematica, 3rd edn. Chapman & Hall/CRC, New York

Publisher's Note Springer Nature remains neutral with regard to jurisdictional claims in published maps and institutional affiliations.

